



# VCU

Virginia Commonwealth University  
VCU Scholars Compass

---

Theses and Dissertations

Graduate School

---

2016

## Cluster Enhanced Nanopore Spectrometry

Amy Chavis

Follow this and additional works at: <https://scholarscompass.vcu.edu/etd>



Part of the [Biological and Chemical Physics Commons](#)

© The Author

---

Downloaded from

<https://scholarscompass.vcu.edu/etd/4290>

This Thesis is brought to you for free and open access by the Graduate School at VCU Scholars Compass. It has been accepted for inclusion in Theses and Dissertations by an authorized administrator of VCU Scholars Compass. For more information, please contact [libcompass@vcu.edu](mailto:libcompass@vcu.edu).

© Amy E. Chavis 2016  
All Rights Reserved

## **Cluster Enhanced Nanopore Spectrometry**

A thesis submitted in partial fulfillment of the requirements for the degree of Master of Science of Physics at Virginia Commonwealth University.

by,

Amy Elizabeth Chavis

Director: Joseph E. Reiner,  
Assistant Professor, Physics Department

Virginia Commonwealth University  
Richmond, VA  
May, 2016

## **Acknowledgment**

The author wishes to thank several people. I would like to thank my friends and family for their constant love and support, especially Elliott Burleson for keeping me well-fed. I would like to thank Christopher Angevine and Kyle Brady for training me and answering my many questions. I would also like to thank my cat, Neko, for the adorable distractions. Last, but not least, I would like to thank my advisor Dr. Joseph Reiner for his enthusiasm, knowledge, guidance, and the opportunity to work on such exciting and interesting research.

## Table of Contents

	<b>Page</b>
<b>Title Page</b> .....	i
<b>Acknowledgment</b> .....	ii
<b>Table of Contents</b> .....	iii
<b>List of Tables</b> .....	vi
<b>List of Figures</b> .....	vii
<b>List of Abbreviations</b> .....	ix
<b>Abstract</b> .....	x
<b>1. Introduction</b> .....	1
1.1. Nanopore sensing and analysis	1
1.1.1. The fundamentals of nanopore detection	1
1.1.2. Biological nanopores	2
1.1.3. The bilayer membrane	5
1.1.4. Applications of single-molecule nanopore sensing	5
1.1.5. Single molecule mass spectrometry	6
1.1.5.1. Polyethylene glycol	8
1.1.6. Sensing peptides and proteins	8

1.2. Thesis Objectives	9
1.2.1. Improving analyte residence time	9
1.2.1.1. Au <sub>25</sub> (SG) <sub>18</sub> enhancement	10
1.2.2. Optimizing Au <sub>25</sub> (SG) <sub>18</sub> enhancement	12
1.2.3. Expanding beyond PEG sensing	12
<b>2. Materials and Methods</b> .....	14
2.1. Analysis using $\alpha$ -hemolysin pores	14
2.1.1. Analysis of PEG	15
2.1.2. Analysis of peptides and PLL	15
2.2. Au <sub>25</sub> (SG) <sub>18</sub> cluster synthesis	16
2.3. The patch-clamp experiment setup, data collection and analysis	17
2.3.1. The hardware	17
2.3.2. Lipid bilayer formation and pore insertion	20
2.3.3. Patch-clamping	20
2.3.4. Data collection	21
2.3.5. Data analysis	21
<b>3. Results</b> .....	23
3.1. Optimizing Au <sub>25</sub> (SG) <sub>18</sub> enhancement	23
3.1.1. Increased transmembrane potential	23
3.1.2. Optimal transmembrane potential	24
3.1.3. Cluster position within the nanopore	26
3.1.3.1. Normalizing residence times over a wide range of PEG sizes	28
3.1.3.2. Optimizing the voltage for cluster-based residence time enhancement	28
3.1.4. PEG on-rate	30
3.1.4.1. Using a correction factor $k_c$	30
3.2. Expanding beyond PEG sensing	33

3.3. Using SMNS for peptide detection	35
3.3.1. Debye screening length	35
3.3.2. Peptide correlation with PEG	37
3.3.3. Peptide enhancement using Au <sub>25</sub> (SG) <sub>18</sub>	38
3.3.4. Altering solution conditions	40
3.3.4.1. Adjusting solution pH	42
3.3.4.2. Adding a denaturing agent	44
3.3.5. Optimizing peptide detection	44
<b>4. Discussion</b> .....	<b>46</b>
4.1. Understanding Au <sub>25</sub> (SG) <sub>18</sub> PEG enhancement	46
4.1.1. Current blockade distribution shift	46
4.1.2. PEG/cluster structural change	50
4.1.3. K <sup>+</sup> interaction with PEG	51
4.2. Modeling the connection between analyte molecular weights and current blockade	52
4.3. Future directions	56
<b>5. Conclusion</b> .....	<b>57</b>
<b>6. References</b> .....	<b>58</b>

**List of Tables**

<b>Table</b>		<b>Page</b>
Table 1	Names of manufacturers and their addresses	14
Table 2	Sequence of peptides used and their molecular weights	34
Table 3	On-rate and residence time of each peptide with and without a gold cluster present	38

**List of Figures**

<b>Figure</b>		<b>Page</b>
Figure 1	Schematic of nanopore detection setup	3
Figure 2	Typical transit event	3
Figure 3	Molecular graph of $\alpha$ -hemolysin	4
Figure 4	$\alpha$ -hemolysin nanopore embedded in planar lipid bilayer	4
Figure 5	PEG mass distributions with a nanopore compared to MALDI-TOF	7
Figure 6	Polyethylene glycol structure	8
Figure 7	Crystalized version of $\text{Au}_{25}(\text{SCH}_2\text{CH}_2\text{Ph})_{18}$	10
Figure 8	Previous $\text{Au}_{25}(\text{SG})_{18}$ enhancement results	11
Figure 9	Instrumental Setup	18
Figure 10	Experimental Apparatus	19
Figure 11	Increasing the transmembrane potential to improve current blockade peak resolution	25
Figure 12	Mean residence times for $\text{PEG}_{28}$ as a function of applied voltage	26
Figure 13	PEG residence times as function of cluster orientation	27
Figure 14	PEG residence times as a function of cluster orientation at varying voltages	29

Figure 15	PEG <sub>28</sub> on-rate kinetics with and without a gold cluster in the nanopore	32
Figure 16	PEG on-rate to a nanopore described by a single exponential functions with and without a gold cluster in the nanopore	32
Figure 17	Poly-L-lysine structure	33
Figure 18	Using SMNS to detect poly-L-lysine	34
Figure 19	Using SMNS to detect peptides	36
Figure 20	Comparing peptide and PEG current blockade peaks vs. molecular weights	37
Figure 21	Using gold clusters to enhance peptide SMNS peptide detection	39
Figure 22	Voltage dependence of cluster enhancement using peptides	39
Figure 23	Noise comparison between PEG and peptides	41
Figure 24	Charge of peptide dependence on solution pH	42
Figure 25	pH dependence on blockade standard deviation and enhancement effect	43
Figure 26	Optimizing peptide detection using SMNS	45
Figure 27	Ohmic model of an $\alpha$ -hemolysin nanopore	47
Figure 28	Current blockade distribution manipulating the interaction term $d$	50
Figure 29	Molecular model of a nanopore	52
Figure 30	Using a calibration curve to describe the correlation between current blockade depth and molecular weight	55

### List of Abbreviations

$\alpha$ HL	alpha hemolysin
FWHM	full width at half maximum
Gdm-HCl	guanidinium hydrochloride
MALDI-TOF	matrix-assisted laser desorption/ionization – time of flight
PAGE	polyacrylamide gel electrophoresis
PEG	polyethylene glycol
PLL	poly-L-lysine
SMMS	single molecule mass spectrometry
SMNS	single molecule nanopore spectrometry

## Abstract

### CLUSTER ENHANCED NANOPORE SPECTROMETRY

By Amy E. Chavis

A thesis submitted in partial fulfillment of the requirements for the degree of Master of Science in Physics at Virginia Commonwealth University.

Virginia Commonwealth University, 2016

Major Director: Joseph E. Reiner, Assistant Professor, Physics Department

Nanopore sensing is a label-free method used to characterize water-soluble molecules. Recent work describes how  $\text{Au}_{25}(\text{SG})_{18}$  clusters improve the single molecule nanopore spectrometry (SMNS) technique when analyzing polyethylene glycol (PEG). This thesis will further study and optimize the enhancement effect resulting from a cluster's presence. Additionally, a model describing the interaction between a cluster and PEG is developed to assist in understanding this mechanism of enhancement. This thesis will also discuss expanding the SMNS method to detect peptides, using  $\text{Au}_{25}(\text{SG})_{18}$  for enhancement, and adjusting solution conditions to improve the sensitivity of the SMNS system for peptide detection. Finally, a model describing the relationship between nanopore current blockades and molecular weight is developed to demonstrate the feasibility of using SMNS as a viable analytical technique for characterizing a wide variety of water-soluble molecules.

## **1. INTRODUCTION**

### **1.1. Nanopore sensing and analysis**

The need for reliable detection of single molecules has become increasingly important in nanobiotechnology,<sup>1</sup> particularly within the field of molecular biology,<sup>2</sup> medical diagnostics,<sup>3</sup> and forensic analysis.<sup>4</sup> Living organisms transport molecules through biological membranes using strictly regulated processes, one of which includes the use of specialized membrane proteins. These transmembrane protein pores are embedded within the biological cell membrane and play an important role in basic biochemical processes. For example, ion channels serve to regulate the flow of specific ions into and out of the cell. Transmembrane pores remaining in a stable and ‘open’ configuration will have very little (or no) selectivity, but they have been shown to serve as nanoscopic current transducers capable of detecting single molecules. These ‘nanopores’<sup>5</sup> allow for real-time visualization of single molecules and their assemblies under biological conditions.<sup>1,5</sup>

#### **1.1.1. The fundamentals of nanopore detection**

Nanopore sensors use an approach similar to the Coulter counter,<sup>6</sup> a device used to count microscale particles, and the classical example of a resistive-pulse sensor.<sup>7</sup> A small aperture separates two electrolyte solutions while a constant ionic current flows through the aperture. Within the electrolyte solution are suspended particles that, upon entering the aperture, will displace a volume of solution equivalent to the volume of that particle. This results in an increase

in the aperture resistance, and a simultaneous reduction in the transaperture current. The concentration of particles suspended in the electrolyte solution can be approximated based on the rate of observed current pulses.<sup>7</sup> Resistive-pulse nanopore detection modifies the Coulter counting principle by reducing the size of the aperture to the nanoscale. The principal of operation is essentially the same where a nanopore is placed between two electrochemical chambers containing salt buffers, separated into *cis* and *trans* compartments (Figure 1), and an applied transmembrane potential drives ionic current through the nanopore. When a molecule accesses the nanopore, this produces a measurable current blockade whose magnitude depends on the ratio of molecular volume to nanopore volume (Figure 2).<sup>5,24</sup>

### 1.1.2. Biological nanopores

The most widely used naturally-occurring biological nanopore is the *Staphylococcus aureus* alpha-hemolysin ( $\alpha$ HL) protein toxin that assembles within a bilayer membrane. This is a mushroom-shaped protein with a hydrophobic  $\beta$ -barrel structure that, when inserted across the membrane, is 100 Å high and up to 100 Å in diameter (Figure 3).<sup>8</sup> It is a heptameric complex that can be divided into three structural domains; the cap, the rim, and the stem. The cap is the widest part of the pore consisting of seven  $\beta$ -sheet pairs and the amino latches of each protomer. The rim domain extends from underneath the heptamer and assists with the pore's stabilization within the membrane.<sup>8,9</sup> The stem domain encompasses the transmembrane channel and in conjugation with the rim domain forms the aromatic amino acid-rich constriction ring. The constriction ring is the narrowest part ( $\sim$ 1.4-1.5 nm)<sup>10</sup> and sets the upper limit for the largest molecules that can be transported through the pore.<sup>8</sup>

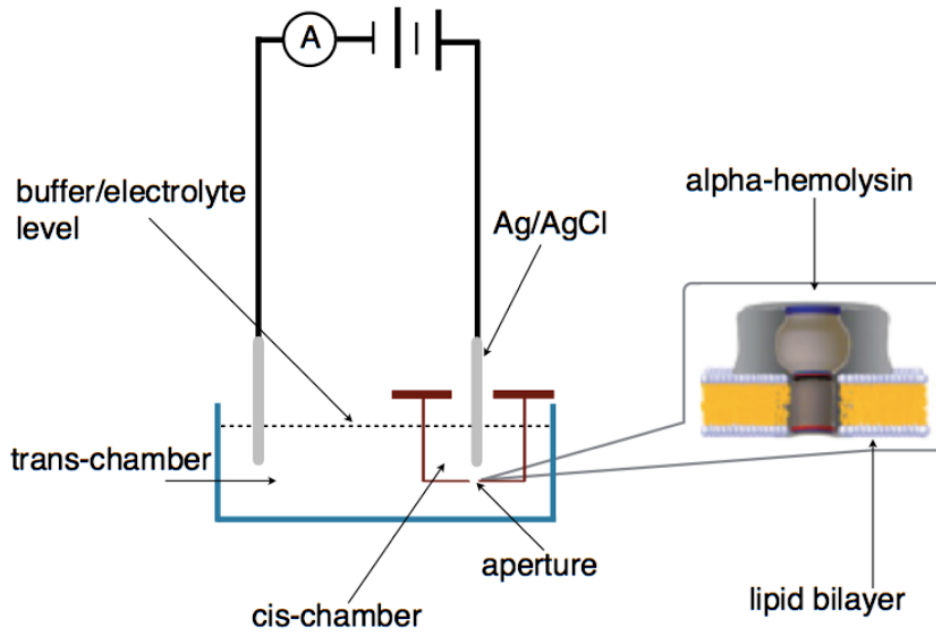


**Figure 1:** Schematic of nanopore detection setup. The patch clamp amplifier is connected to two Ag/AgCl electrodes placed on either side of an aperture separating the *cis*-chamber (red) from the *trans*-chamber (blue). The aperture contains nanopores inserted into a planar lipid bilayer membrane ( $\alpha$ HL here).

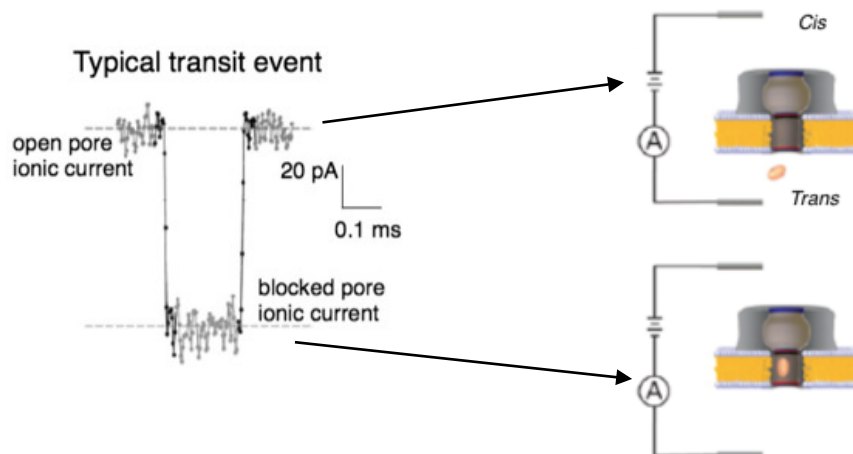


**Figure 2:** A typical transit event. Current flows through an open nanopore yielding an average open pore current. If a molecule enters the pore, the ionic current will reduce and yield an average ionic current blockade. (Reprinted with permission from [28])

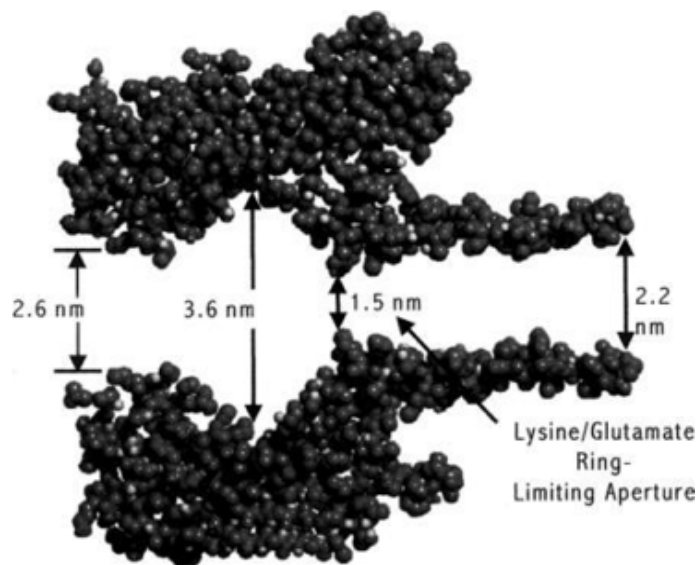


**Figure 3:** Molecular graph of alpha hemolysin nanopore. Dimensions of various regions of the lumen of the pore are provided. (Reprinted with permission from [10])

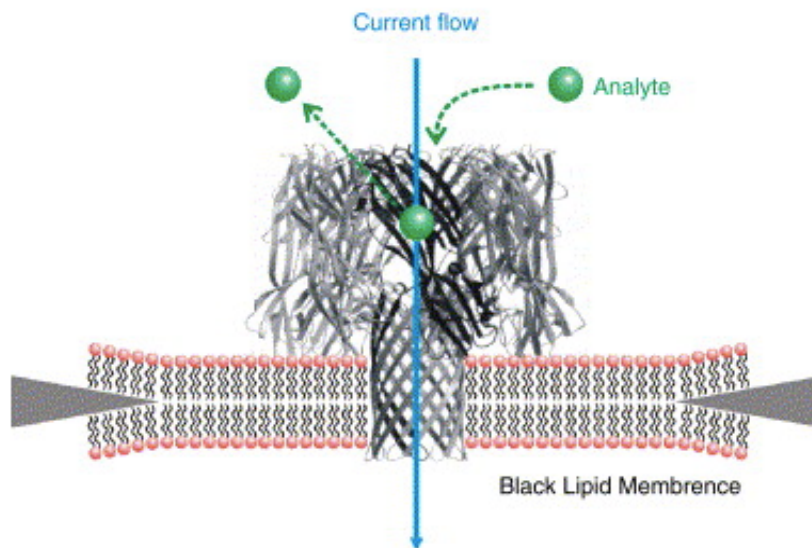


**Figure 4:**  $\alpha$ HL nanopore embedded in a planar lipid bilayer (black lipid membrane). The phospholipid membrane extends approximately 100  $\mu\text{m}$  in a hydrophobic support. The path of cis-side entry analytes are shown through the lumen of the nanopore. (Reprinted with permission from [14])

### 1.1.3. The bilayer membrane

The natural environment for a membrane protein to assemble is a lipid bilayer membrane, a fluid-like self-assembled structure ~5 nm thick (Figure 4).<sup>11</sup> Meuller *et al.* observed the formation of a planar lipid bilayer which was called a ‘black lipid membrane’ based on its appearance using optical microscopy.<sup>12,13</sup> The membrane consists of amphiphilic lipid molecules across an aperture separating two chambers containing aqueous solutions. The lipid molecules will orient themselves into a bilayer structure with the hydrophilic head group of the lipid molecules pointing into the aqueous exterior region and the hydrophobic tail portion of the molecule oriented towards the interior.<sup>14</sup> These membranes can be formed in laboratories as freestanding, nearly perfect insulating planar membranes ( $R_{\text{membrane}} > 10\text{-}100 \text{ G}\Omega$ ) and provide a stable environment to support  $\alpha$ HL channels.<sup>11</sup>

### 1.1.4. Applications of single-molecule nanopore sensing

Nanopore-based sensor research has a wide range of useful biological applications.<sup>15</sup> DNA and RNA sequencing using nanopores has become increasingly important to diagnose and monitor various diseases.<sup>16,17</sup> Manrao *et al.* demonstrated the ability to resolve changes in current that correspond to a DNA sequence translocating through a nanopore.<sup>18</sup> Wang *et al.* detected an abundance of circulating microRNAs corresponding to a lung cancer diagnosis.<sup>17</sup> By hybridizing a complimentary probe to a target miRNA, the complex was allowed to translocate through a nanopore. Detecting various protein folding patterns can also be used in disease diagnosis, and nanopores can be used as a real-time monitoring device. Hu *et al.* investigated the two structural features in the amyloidosis process using a characteristic nanopore blockade event to decipher between a random coil and a  $\beta$ -sheet structure.<sup>19</sup> The excessive self-assembly of this particular

peptide ( $\beta$ -amyloid) in the brain is associated with Alzheimer's disease. Nivala *et al.* used the AAA+ unfoldase ClpX to assist in protein translocation through a nanopore.<sup>20</sup> It was found that characteristic blockade states could be linked to unfolding events in various proteins. Their results demonstrate that a molecular motor like ClpX can drive proteins through nanopores and assist with future protein translocation studies.

### 1.1.5. Single molecule mass spectrometry

Using nanopores as sensors originated when researchers attempted to characterize the geometry of nanoscale transmembrane pores.<sup>21,22</sup> Various sizes of the common molecule polyethylene glycol (PEG) were used by Merzlyak *et al.*<sup>23</sup> to estimate pore diameters and geometries. Krasilnikov *et al.*<sup>24</sup> demonstrated that increasing the ionic strength of the electrolyte solution increased the mean residence time of PEG in the biological pore alpha hemolysin ( $\alpha$ HL), which enabled one to detect measurable current blockades from individual molecules. Robertson *et al.*<sup>25</sup> then created a histogram of the averaged current from each of these blockades, which showed distinct peaks corresponding to PEG molecules differing in size by a single monomer unit (Figure 5A).<sup>25,26,27,28,68</sup> The mPEG histogram has a 1:1 correspondence to a MALDI-TOF mass spectrogram for the same pPEG sample (Figure 5B), which motivated the use of the term “single molecule mass spectrometry” (SMMS) to describe this technique.<sup>25,27,28</sup> However, the SMMS technique cannot measure particle mass independent of size; therefore, this technique will be referred to hereafter as “single molecule nanopore spectrometry” (SMNS).

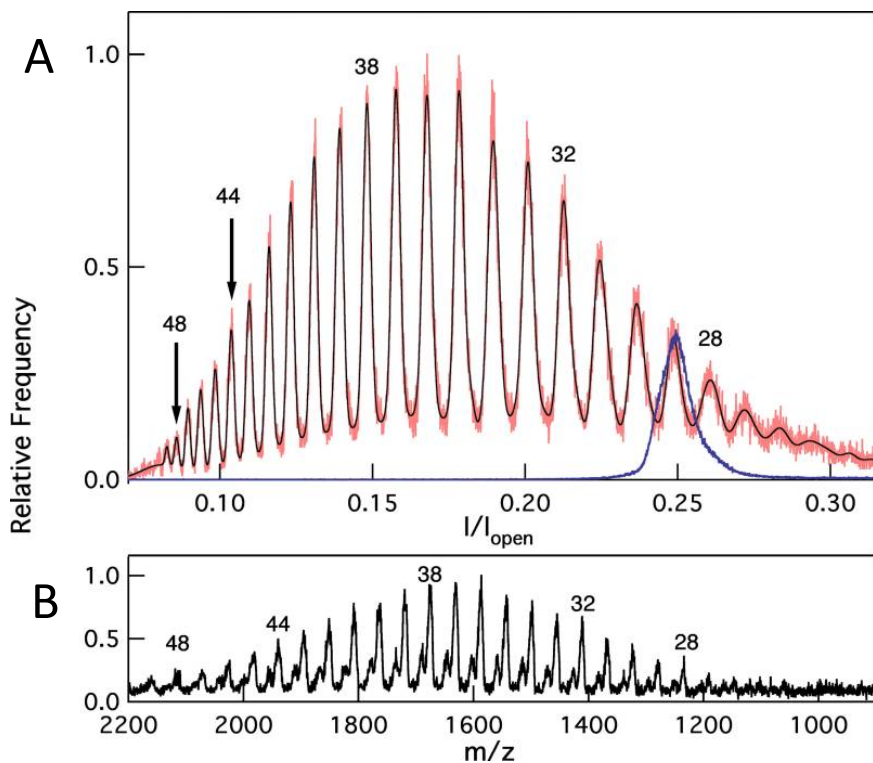


**Figure 5:** Roberston *et al.* mass distributions using a single nanopore compared to a MALDI-TOF mass spectrum for polydisperse PEG ( $M_r=1,500$  g/mol). Histogram peaks correspond to PEG molecules difference in size by a single monomer unit (44 g/mol). **(A)** Larger values of  $I/I_{open}$  correspond to lower PEG molecular masses, and smaller values of  $I/I_{open}$  correspond to high PEG molecular masses. **(B)** MALDI-TOF mass spectrum. (Reprinted with permission from [25], Copyright (2007) National Academy of Sciences, U.S.A.).

### 1.1.5.1. Polyethylene glycol (PEG)

PEG is a common neutral polymer that is water-soluble and can be branched or linear.<sup>29</sup> It has an important history in nanopore sensing as shown in Section 1.1.5., but also plays an important role in many other biotechnical and biomedical applications like: peptide and protein stabilization,<sup>30</sup> drug delivery,<sup>31</sup> green chemistry,<sup>32</sup> nanoparticle surface modification,<sup>33</sup> synthesis,<sup>34</sup> catalysis,<sup>35</sup> and stabilization of nanometer sized gold clusters.<sup>36</sup> There are a large number of PEG applications associated with stabilized metallic clusters<sup>37</sup> motivating the study of interactions between clusters and PEG. Additionally, PEG is non-toxic and available in a variety of molecular weights (Figure 6).<sup>29</sup>

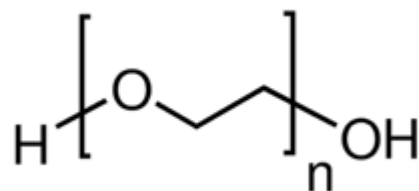


**Figure 6:** Polyethylene glycol structure where  $n$  indicates the degree of polymerization.  $MW_{PEG} = (44 \text{ g/mol})n + 12 \text{ g/mol}$  (<http://www.sigmaaldrich.com>).

### 1.1.6. Sensing peptides and proteins

Research has shown the ability to detect proteins using glass nanopores,<sup>38</sup> nanofabricated chips,<sup>39</sup> solid state nanopores,<sup>40</sup> or binding proteins to ssDNA.<sup>41</sup> However, due to their size, proteins are unable to translocate through biological nanopores like  $\alpha$ -hemolysin and can be difficult to detect. Sutherland *et al.* first demonstrated that peptide analysis through a biological nanopore was possible using different repeat units of a collagen-like sequence.<sup>42</sup> It was also found that peptides, containing more repeat-units, yielded longer-lived and deeper blockades.<sup>43</sup> The enzyme Trypsin has been utilized to cleave polypeptides, which enable smaller peptides to

translocate through the nanopore.<sup>44,45</sup> Small, naturally-occurring peptides have physiological applications, and a growing number of small peptides are being utilized in the biopharmaceutical industry.<sup>46,47</sup> SMNS could benefit biomedical research by providing a real-time, sensitive, and cost-effective approach to further understand the properties of peptides. More effort is being focused on peptide detection with nanopores<sup>48,49,50</sup> and a better understanding of the nature of nanopore-based peptide detection is crucial for this effort. For example, current studies focus on detecting known peptides in solution,<sup>51,52,53</sup> but it would be more advantageous if one could detect a number of unknown peptides in real time and assign each current blockade to a particular peptide. This is not currently possible, but it is a long-term goal of this research.

## **1.2. Thesis Objectives**

### **1.2.1. Improving analyte residence time**

The SMNS technique requires an analyte to reside within the nanopore for an extended period of time. This will decrease the standard of error of the estimated average from each blockade, eventually resulting in a clearer current blockade distribution. As previously stated, increasing the ionic strength of the electrolyte solution increases the PEG residence time in the  $\alpha$ -hemolysin pore. This will enable the current blockade distribution to mimic a mass spectrum; however, this will not increase most analyte residence times.<sup>54</sup> Other researchers have modified the physical characteristics of the solution to increase analyte residence times. Fologea *et al.* and Kowalczyk *et al.* demonstrated increased DNA residence time by reducing the solution temperature, increasing solution viscosity, and using different counterions.<sup>54,55</sup> However, in some cases the ionic conductivity and analyte on-rate was reduced,<sup>56</sup> which decreases the quality and sensitivity of analysis.

### 1.2.1.1. Au<sub>25</sub>(SG)<sub>18</sub> enhancement

More sophisticated methods are being used to improve analyte residence times. Previously, negatively charged metallic clusters were utilized to increase cationic analyte residence times.<sup>57</sup> Au<sub>25</sub>(SG)<sub>18</sub> is an anionic, glutathione (C<sub>10</sub>H<sub>17</sub>N<sub>3</sub>O<sub>6</sub>S) protected, water-soluble gold cluster.<sup>58,59,60,61,62,63,64</sup> The diameter of this cluster has not been characterized in solution; however, a similarly-sized cluster Au<sub>25</sub>(SCH<sub>2</sub>CH<sub>2</sub>Ph)<sub>18</sub> has been crystalized (Figure 7) and shown to have a diameter of 2.4 nm.<sup>58</sup> Figure 8b shows that under an applied electric field, the cluster can be driven into the *cis*-side vestibule of an  $\alpha$ -hemolysin pore and remain for extended periods (>10 seconds). This partially blocks the ionic current by about 25%, allowing PEG molecule to enter the *trans*-side of the  $\alpha$ -hemolysin pore and yield sizable current blockades. The cluster-PEG interaction increased PEG residence time by an order of magnitude yielding higher resolution peaks in the current blockade distribution (Figure 8c).

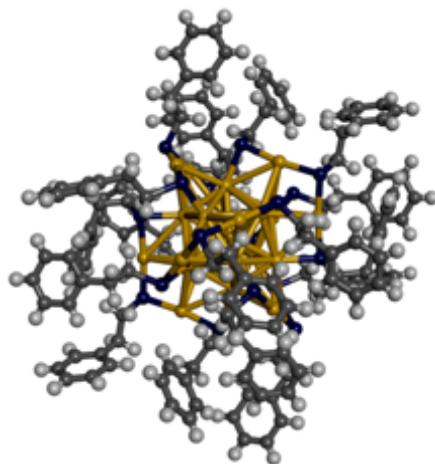


**Figure 7:** Crystalized version of Au<sub>25</sub>(SCH<sub>2</sub>CH<sub>2</sub>Ph)<sub>18</sub> included for visualization purposes. Au<sub>25</sub>(SG)<sub>18</sub> has a similar size (~2.4 nm). (Image created by Anthony F. Pedicini (VCU, Richmond, VA) using Discovery Studio 4.1)

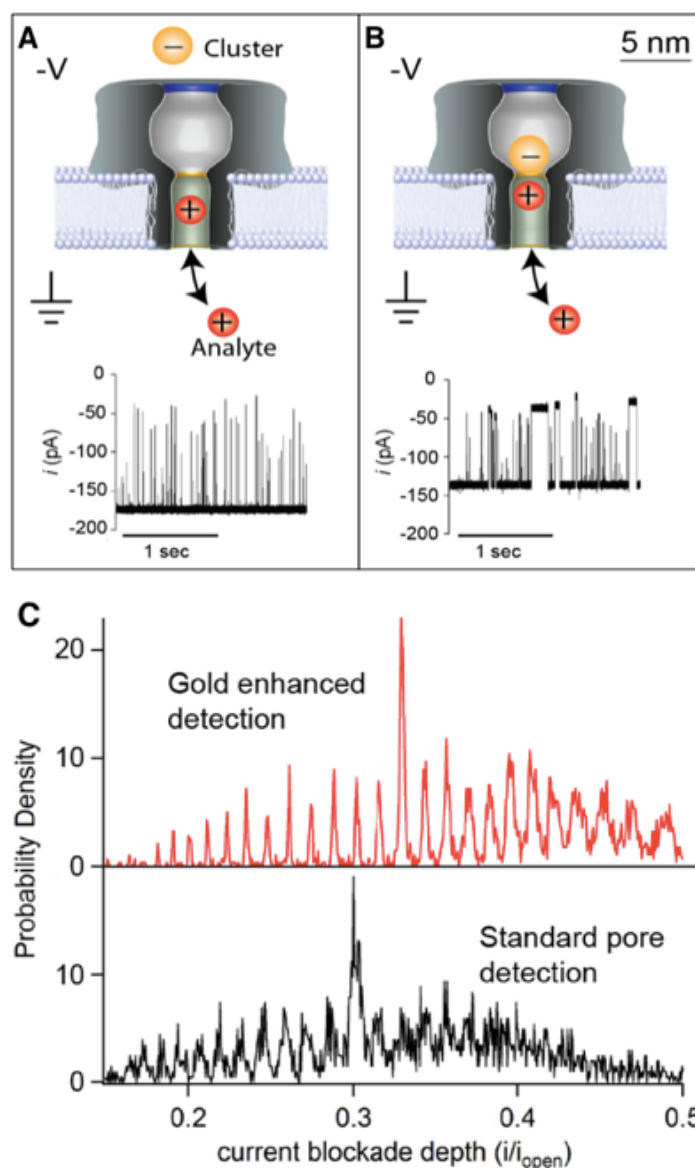


**Figure 8:** Previous  $\text{Au}_{25}(\text{SG})_{18}$  enhancement results: **(A)** A PEG molecule enters from the *trans*-side of the  $\alpha$ HL pore and gives rise to short-lived current blockades. **(B)** Gold clusters diffuse and enter from the *cis*-side, decreasing the current for extended periods of time. The PEG molecule yields longer-lived blockades in the presence of a gold cluster. **(C)** A distribution of normalized PEG current blockades shows peaks corresponding to different sized molecules. The presence of gold clusters increases PEG residence times resulting in narrower peaks (red) and a more accurate characterization of the analyte in comparison to peak distributions with PEG alone in pore (black).<sup>57</sup>

### **1.2.2. Optimization of Au<sub>25</sub>(SG)<sub>18</sub> enhancement**

This thesis will show improvements in optimizing the residence time enhancement between PEG molecules and thiolate-capped gold clusters, and characterize their interaction. The PEG-cluster interaction is shown to have a dependence on the applied transmembrane voltage and cluster blockade states. Additionally, a model is presented showing the interaction between PEG and the cluster inside the pore. This model accurately describes the shift in the current blockade peak positions occurring when a cluster is present within a nanopore. These results indicate optimal conditions for utilizing clusters in SMNS technology, further suggesting SMNS as a useful tool to quantify metal-polymer interactions within a nanoconfined environment.<sup>65</sup>

### **1.2.2. Expanding beyond PEG sensing**

This thesis will also move beyond PEG and explore using the SMNS approach for other analytes. It is shown that poly-L-lysine (PLL) also exhibits the same characteristic comb-like blockade peaks seen with PEG and can be treated as such. The SMNS process is then used to analyze various peptides, resulting in characteristic blockade peaks and residence times that are consistent with PEG results in similar conditions. Additionally, a model is created to correlate molecular weights with current blockade depths.

Improvements in the SMNS sensing capabilities of peptides are also investigated here. As seen with PEG, metallic clusters are shown to increase the residence time of peptides within a nanopore. However, unlike PEG, peptides exhibit a larger degree of noise within the pore that may result from secondary structures not present in PEG molecules. With this in mind, the role that various solution conditions play on the standard deviation of each blockade is investigated and it is shown that by reducing these fluctuations, the peptide-induced current blockade peaks are

further resolved. Overall, it is shown that the combination of a gold cluster in the nanopore and adjustments to solution conditions improve the resolution of peptide-based current blockade distributions to levels commensurate with PEG.

## 2. MATERIALS AND METHODS

**Table 1:** This table shows the names of the manufacturing companies for equipment, supplies and reagents used in this thesis, and their addresses.

Company	Address
Avanti Polar Lipids Inc.	Alabaster, AL, USA
Axio Observer	Zeiss, Germany
Eastern Scientific	Rockville, MD, USA
Eppendorf North America	Hauppauge, NY, USA
Kinetic Systems	Boston, MA, USA
List Biological Laboratories Inc.	Campbell, CA, USA
Molecular Devices	Carlsbad, CA, USA
National Instruments	Austin, TX, USA
Polypure	Oslo, Norway
Scientific Specialists	Baltimore, MD, USA
Sigma-Aldrich	St. Louis, MO, USA
Sutter Instrument	Novato, CA, USA
Thermo Scientific	Waltham, MA, USA
Wavemetrics Inc.	Lake Oswego, OR, USA
World Precision Instruments (WPI)	Sarasota, FL, USA

### 2.1. Analysis using $\alpha$ -hemolysin pores

The  $\alpha$ -hemolysin solution used in all experiments performed in this thesis was created by adding 0.5 mL millipore water (18 M $\Omega$ ·cm) to 0.25 mg Alpha Toxin from *Staphylococcus aureus* purchased from List Biological Laboratories Inc. This was then aliquoted into several protein lo-bind tubes (Eppendorf) and stored in a -80 °C freezer (Thermo Scientific).

The stock lipid solution used in all experiments was made by adding 500  $\mu\text{L}$  hexadecane (Sigma-Aldrich) to 5 mg 1,2-diphytanoyl-*sn*-glycero-3-phosphocholine purchased from Avanti Polar Lipids Inc. This was then aliquoted into 5 (1/2 dram) glass vials (Scientific Specialists) and stored in a  $-20\text{ }^{\circ}\text{C}$  freezer.

The stock prepaint solution was created by adding 500  $\mu\text{L}$  pentane (Sigma-Aldrich) to 5 mg 1,2-diphytanoyl-*sn*-glycero-3-phosphocholine purchased from Avanti Polar Lipids Inc. This was then aliquoted into 5 (1/2 dram) glass vials and 900  $\mu\text{L}$  of pentane was added to each vial. Vials were store in  $-20\text{ }^{\circ}\text{C}$  freezer.

A transmembrane potential was applied through Ag/AgCl electrodes and experiments were performed as described in Section 2.3. All experiments were carried out at  $21 \pm 2\text{ }^{\circ}\text{C}$ .

### **2.1.1. Analysis of PEG**

The electrolyte solution used for the PEG in KCl measurements (Section 3.1.) was 3.5 M KCl in 10 mM Tris buffer (pH 7.2). The reference tip contained 3.5 M KCl buffer and 40  $\mu\text{M}$   $\text{Au}_{25}(\text{SG})_{18}$ . PEG concentrations and transmembrane potential are specified in each figure description. The LiCl comparison study (Section 4.1.3.) used 3 M LiCl and 3M KCl, with an applied transmembrane potential of 50 mV and 5  $\mu\text{M}$  PEG<sub>28</sub> in the *trans* compartment.

### **2.1.2. Analysis of PLL and peptides**

The electrolyte solution used for the PLL study (Section 3.2) was 2.5 M KCl in 10 mM Tris buffer (pH 7.2), with an applied transmembrane potential of 50 mV. The reference tip contained 2.5 M KCl buffer, and the *trans* compartment contained 20  $\mu\text{M}$  PLL.

The electrolyte solution used for the peptides study (Section 3.3) was 3.0 M KCl in 10 mM Tris buffer, with a pH of 7.2 (Figures 19,20,21,22,23) or varying pH's (Figure 24,25). Each peptide study was performed independently of each other, using 20  $\mu$ M of each peptide in the *trans* compartment. Unless otherwise stated, all peptide studies had an applied transmembrane potential of 70 mV.

## 2.2. Au<sub>25</sub>(SG)<sub>18</sub> Cluster Synthesis

Au<sub>25</sub>(SG)<sub>18</sub> clusters were obtained through collaboration with Dr. Amala Dass's laboratory from the Department of Chemistry and Biochemistry at the University of Mississippi using the following methodology.

100 mg of HAuCl<sub>4</sub> (0.253 mM/L) was dissolved in 50mL of DI water, resulting in a yellow solution. 307 mg of glutathione (1.00 mM/L) was slowly added to the gold salt under slow stirring, while the yellow solution changed to a cloudy white suspension. Next the solution was cooled in an ice bath for 30 min. Afterwards, 94.6 mg of NaBH<sub>4</sub> (2.5 mM/L) was dissolved in 12.5 mL of ice cold DI water and added to the mixture all at once while stirring at 1000 rpm. The milky white color of the mixture rapidly turned black after the addition of NaBH<sub>4</sub>, indicating the formation of nanoparticles. After 1 hour, the mixture was rotary evaporated until the total volume was reduced to 5 mL, while the temperature was kept below 30 °C. Then 20 mL of methanol was added to the product mixture and centrifuged at 3800 rpm for 3 min. The resulting precipitate was washed three times with methanol. Au<sub>25</sub>(SG)<sub>18</sub> was obtained using polyacrylamide gel electrophoresis (PAGE-as described previously).<sup>66</sup>

## 2.3 The patch-clamp experiment setup, data collection and analysis

### 2.3.1. The hardware

The investigation of individual PEG and peptide molecules with  $\alpha$ -hemolysin pores was conducted using patch-clamp apparatus. Figures 9-10 show photographs of the instrumental setup. The patch-clamp instrument consists of four main components connected to a computer: the holder/Teflon unit, the electrodes, the amplifier, and the digitizer.

The holder/Teflon unit consists of a 1 cm<sup>2</sup> polytetrafluoroethylene (PTFE, Teflon) sheet with a ca. 100  $\mu$ m hole in the center (Eastern Scientific). This is fixed to a previously fabricated large holder with polydimethylsiloxane (PDMS, Kwik-Cast, WPI) separating the holder/Teflon unit into two compartments, *cis* and *trans*. The compartments have approximate volumes of 650  $\mu$ L (*cis*) and 2500  $\mu$ L (*trans*). The holder positions the Teflon sheet ca. 300  $\mu$ m from the top of the microscope coverslip mounted onto a homemade base that sits on an inverted microscope (Axio Observer). The microscope is bolted to an air-floated optical table within a Faraday cage enclosure (Kinetic Systems) to reduce vibrational interference of the signal and protect against external electric noise.

The electric potential across the lipid bilayer is applied via two Ag/AgCl electrodes that had been prepared by sanding silver wire and holding in bleach for  $\sim$ 1 hour prior to each experiment. The measuring electrode is connected to the *trans* compartment and the reference electrode is connected to the *cis* compartment.

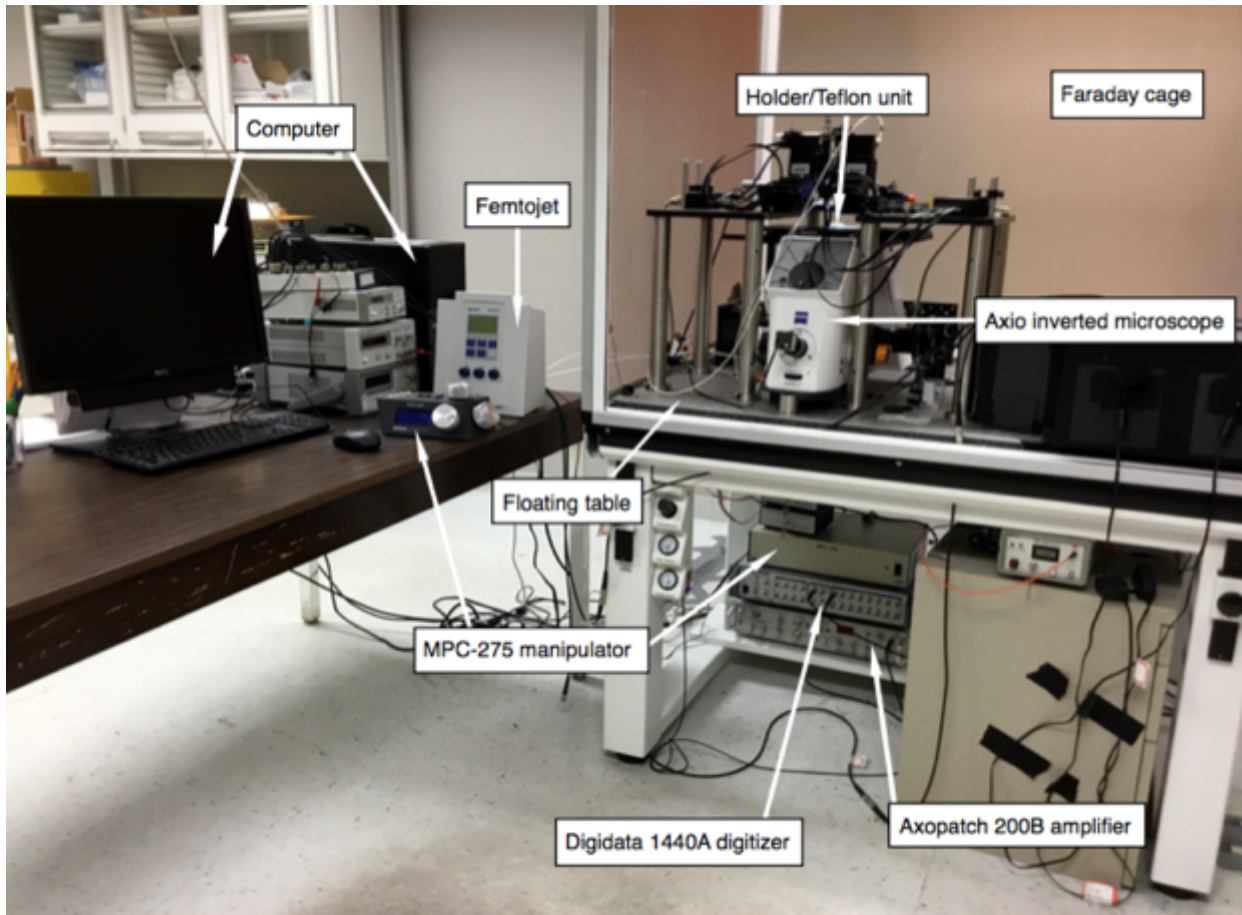


**Figure 9:** Instrumental Setup. All hardware used in the experimental process is labeled.

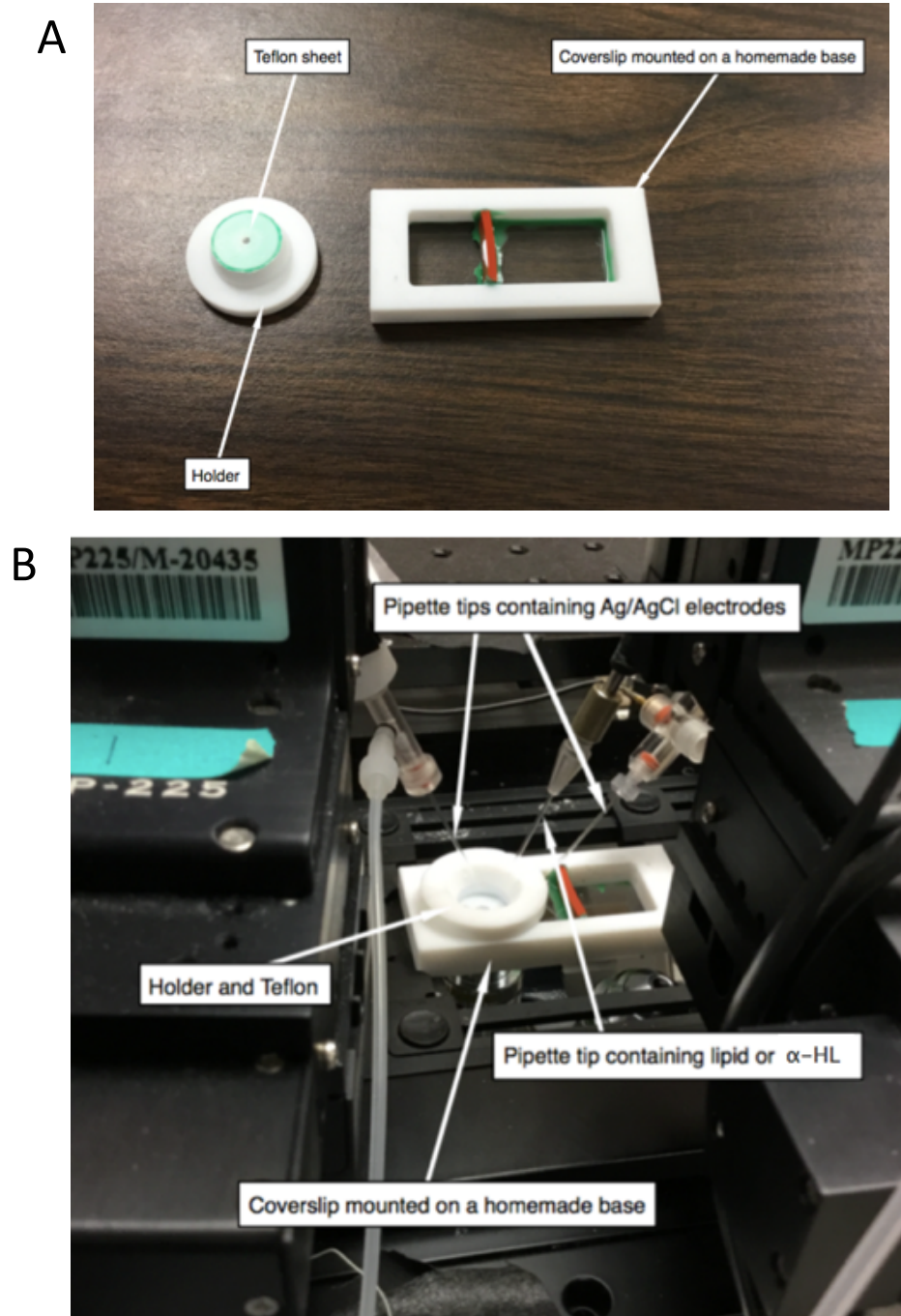


**Figure 10:** Experimental Apparatus. **(A)** Holder/Teflon unit and base deconstructed. **(B)** Holder/Teflon unit set into base and onto the inverted microscope. Pipette tips are shown in their respective holders and inserted into solution.

### 2.3.2. Lipid Bilayer formation and pore insertion

The preprint mixture is applied to both sides of the 100  $\mu\text{m}$  hole after attachment to the holder. The holder is then placed into the base and *cis* and *trans* compartments of the unit are filled with their respective electrolyte/buffer solution. Membranes are formed with a painting methodology closely related to the method of Mueller *et al.*<sup>13</sup> A borosilicate capillary (1 mm OD, 0.78 mm ID with filament, Sutter Instrument) pipette tip is formed with a laser-based pipette puller (P-2000, Sutter Instrument) and filled with lipid solution. This is positioned with a motorized manipulator (MPC-275, Sutter Instrument) just above the Teflon partition. Several picoliters of lipid solution are ejected under pressure (Femtojet, Eppendorf) from the tip and adhere to the Teflon surface. A glass rod with a ball formed at the tip is manipulated with a manual translation stage to wipe the lipid across the hole. The lipid/solvent mixture thins under an applied voltage ( $\sim 100$  mV) and a lipid bilayer membrane is formed. The membrane formation process is verified with bright-field optical microscopy.

After the membrane is formed, a second pipette tip containing  $\alpha$ -hemolysin is positioned above the bilayer and a backing pressure ( $\sim 15$  hPa) is applied for several seconds. A transmembrane voltage (20 mV) is applied to verify and encourage pore insertion. When a sufficient number of pores (ca. 500) are in the membrane, the backing pressure is turned off and the tip is removed from solution.

### 2.3.3. Patch-clamping

A quartz capillary (1 mm OD, 0.7 mm ID with filament, Sutter Instrument) patch pipette tip is filled with the same buffer solution used in *cis* and *trans* side plus 40  $\mu\text{M}$   $\text{Au}_{25}(\text{SG})_{18}$ . A Ag/AgCl electrode is inserted into the pipette to enable the application of a transmembrane

potential. This pipette is brought down onto the membrane to isolate a single channel within a patch. If the patch membrane contains zero or more than one  $\alpha$ -hemolysin pore it is removed from the surface and backing pressure is applied to remove the patch. The process is repeated until a single channel is isolated at the end of the electrode tip. The number of attempts required to obtain a single channel depends predominantly on the concentration of pores in the membrane. For our experimental parameters we typically capture a single pore every 5-10 patching attempts. The presence of a single pore can be determined by comparing the time-averaged current with the expected single channel current. For example, a single pore in 3.5 M KCl at pH 7.2 we expect a conductance of 3.2 nS.<sup>67</sup>

#### **2.3.4. Data Collection**

Ionic currents are recorded using an amplifier head stage with a four-pole 10 kHz low-pass Bessel filter (Axopatch 200B, Molecular Devices) sampled at 50 kHz (Digidata 1440A, Molecular Devices). The patch-clamp instrument is connected to a computer that records data in axon binary files (.abf) using Clampex software included in the pClamp 10 package (Molecular Devices).

#### **2.3.5. Data Analysis**

Data analysis of the .abf files are performed with in-house software written in Labview 8.5 (National Instruments). A threshold algorithm, similar to one described by Reiner *et al.*,<sup>28</sup> was used to calculate the average blockade depth and residence time for each event. The average blockade depth associated with a gold cluster is about 25%. In order to avoid confusion between gold cluster and PEG-induced blockades, the current blockade threshold was set to detect events that remain 35% above the open-pore current for a minimum period of 140  $\mu$ s. This allows for analysis of

current blockades from both the open-nanopore state and the gold-blocked state for the same pore. The average current for each blockade was normalized by the average open current 1 ms before and 1 ms after the blockade event. Blockade events were discarded if the averaged open-state current fell outside of a narrow window defined as full width at half maximum of the open-pore current distribution, and full width at half maximum of the largest peak in the cluster-occupied current distribution. The  $n$ -values for each peak in the blockade distributions (Figure 11) were calibrated by assigning  $n = 28$  to the largest peak.<sup>25,28,68</sup>

The residence time for each event was defined as the period 20  $\mu$ s before the initial threshold crossing (initiation of a blockade) to 20  $\mu$ s (completion of a blockade). The residence time for a given blockade was assigned to PEG $_n$  molecule (PEG with  $n$ -monomer repeat units) if the magnitude of the current blockade fell between the two minima surrounding the  $n$ -th peak in the current blockade distribution. Ten-bin histograms (automatic bin widths) were calculated from the residence times for each PEG $_n$  using the histogram analysis package in IGOR 6.22A (Wavemetrics Inc.).

The residence time distribution of events corresponding to PEG $_n$  are well fit by single-component exponential functions from which the time constant for a given PEG $_n$  is referred to as the mean residence time. The quality of the current blockade distributions was quantified by the peak resolution ( $R_n = 1.18(\mu_n - \mu_{n-1})/(\sigma_n + \sigma_{n-1})$ ), where  $\mu_n$  is the location of the PEG $_n$  peak in the distribution and  $\sigma_n$  is the standard deviation of the PEG $_n$  peak. The resolution characterizes the spacing between adjacent peaks relative to the peak widths. Baseline resolved peaks correspond to  $R_n \approx 1$  and peak quality improves with increasing  $R_n$  values.<sup>57</sup>

### 3. RESULTS

#### 3.1. Optimizing Au<sub>25</sub>(SG)<sub>18</sub> enhancement

##### 3.1.1. Increased Transmembrane potential

It has been hypothesized that there is a Coulombic attraction between cationic PEG and the anionic Au<sub>25</sub>(SG)<sub>18</sub> cluster. If the Coulombic attraction is responsible for lengthening PEG's residence time within a nanopore, then increasing the transmembrane potential across the membrane will further increase PEG's residence time. In this case, the applied electric field is forcing a stronger interaction between PEG and the cluster when they are both within the pore volume. As was shown previously, an increase in PEG residence time leads to improved peak resolution in terms of the current blockade distribution (Section 1.2.1.).<sup>57</sup> So it follows that increasing the transmembrane potential would further improve the PEG residence times when gold is present within the pore, thus enhancing the resolution of the peaks in the gold-occupied current blockade distribution. Resolution is defined as,

$$Resolution = \frac{\textit{spacing between peaks}}{\textit{width of peaks}}$$

so that the ultimate goal would be to decrease the width of each current blockade peak. Figure 11 shows that an increase in transmembrane potential through a gold-occupied nanopore from 50 mV to 60 mV improves the resolution of the current blockade distributions. PEG<sub>30</sub>'s peak resolution in a gold-occupied pore improved by 37%. ( $R_{30\text{-gold}}(50 \text{ mV}) = 2.07$  and  $R_{30\text{-gold}}(60 \text{ mV}) = 2.84$ ). In

contrast, a cluster free pore decreased PEG<sub>30</sub>'s peak resolution by 20% ( $R_{30\text{-open}}(50\text{ mV}) = 1.24$  and  $R_{30\text{-open}}(60\text{ mV}) = 1.03$ ).<sup>69</sup>

### 3.1.2. Optimal transmembrane potential

It is clear that the quality of the PEG-induced current blockade distribution partially depends on the mean residence time of the molecule within the pore. Based on this, an optimal voltage for cluster-enhanced SMNS can be determined by measuring the mean residence time of PEG<sub>28</sub> in both the open-pore and gold-occupied configurations as a function of applied voltage. In the open-pore configuration, the mean residence time decreases monotonically with increasing voltage (Figure 12, inset).<sup>28,70</sup> In this configuration, PEG residence time peaks around 40 – 50 mV, agreeing with previous reports that show a non-trivial dependence between applied voltage and PEG residence time.<sup>70,71</sup>

If a gold cluster is present in the pore, then PEG's mean residence time also follows a non-trivial dependence on the applied voltage. Increasing the voltage does show in a stronger interaction between PEG<sub>28</sub> and a cluster, resulting in a peak mean residence time of PEG<sub>28</sub> occurring near the applied voltage of 60 mV (Figure 12). However, further increasing the transmembrane potential beyond 60 mV causes a reduction in PEG<sub>28</sub> residence time. One reason for this observation is that larger potentials tend to remove cations bound to PEG<sub>28</sub>, thus weakening the residence time enhancement mechanism.<sup>28</sup>

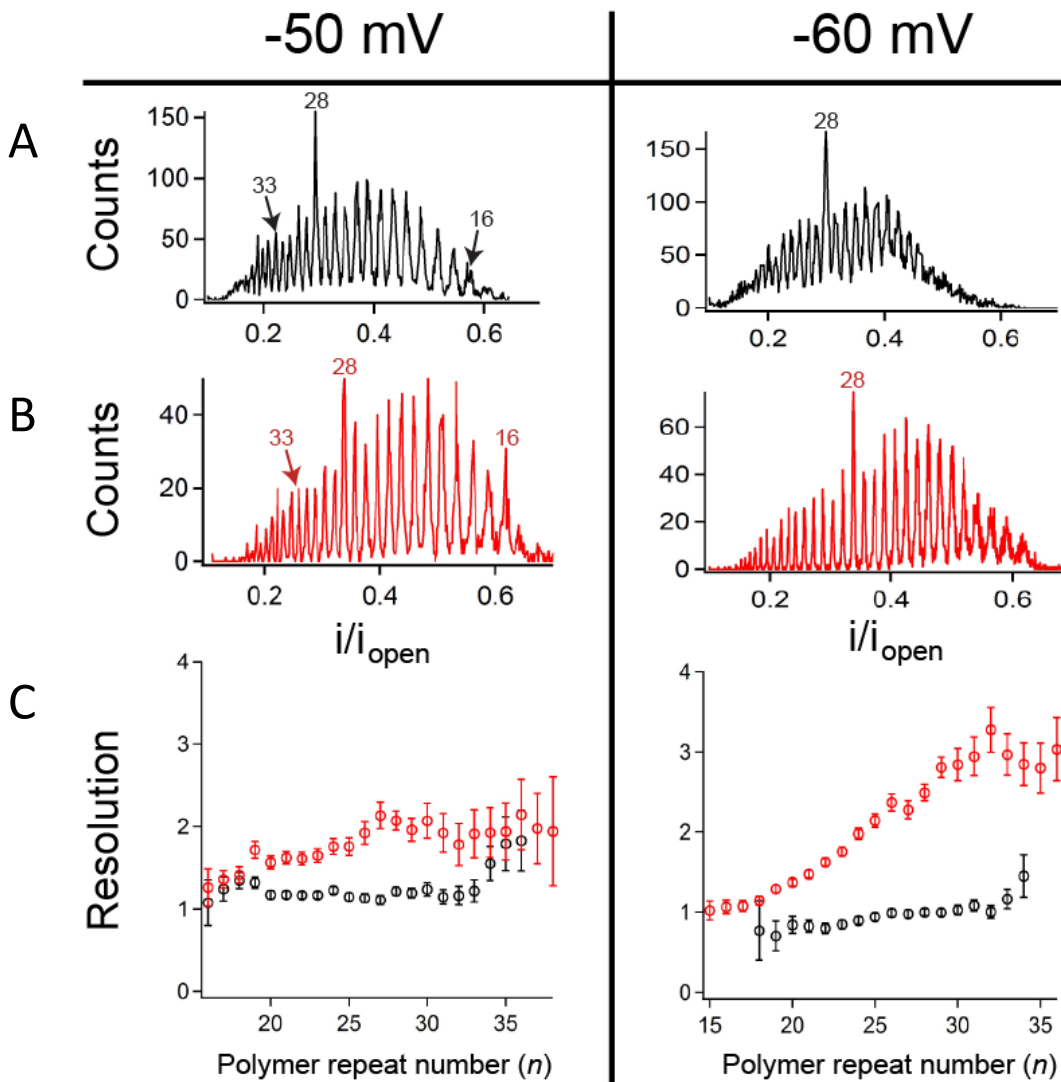


**Figure 11:** Increasing the transmembrane potential with a gold cluster present increases peak resolution of the PEG-induced current blockade distribution. **(A)** PEG induced blockade for the open-pore configuration with an applied transmembrane potential of 50 mV (left) and 60 mV (right). **(B)** Improvements in the resolution of PEG induced blockades for the cluster-occupied configuration with an applied transmembrane potential of 50 mV (left) and 60 mV (right). **(C)** The open pore blockade distribution (black) degrades with an increase in transmembrane potential. If a gold cluster occupies the pore, then there is an improvement in resolution (red). This data was recorded using 10  $\mu\text{M}$  polydisperse PEG-1000, 10  $\mu\text{M}$  polydisperse PEG-1500 and 1  $\mu\text{M}$  PEG<sub>28</sub>.<sup>69</sup>

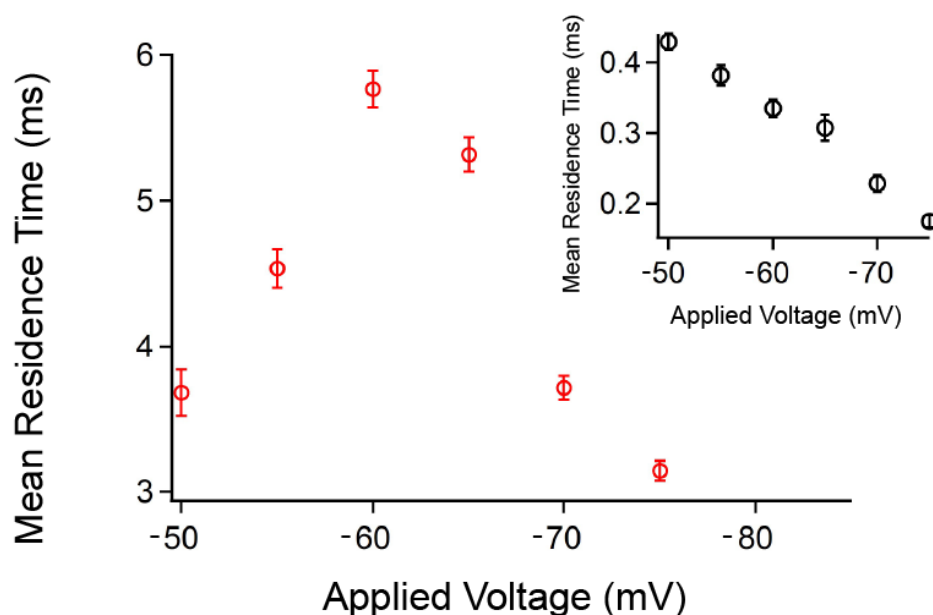


**Figure 12:** Mean residence times for PEG<sub>28</sub> as a function of the applied voltage in the open (black) and gold-occupied (red) pore. The mean residence time with gold present increases with increasing transmembrane potential until a peak at 60 mV, then a steady decrease at higher voltages (inset). The open pore configuration decreases in mean residence time over the entire range of voltages. Error bars correspond to  $\pm 1$  S.D. This data was recorded using 10  $\mu$ M PEG<sub>28</sub>.<sup>69</sup>

### 3.1.3. Cluster position within the nanopore

If the interaction between the cluster and PEG play an important role, then the cluster's position and orientation within the pore would have an effect on analyte residence time. If the bulk of the gold cluster is situated on top of the constriction ring, or closer to the *trans*-side of the pore, then it will interact more strongly with PEG located in the *trans*-side lumen. Clusters located in this position will also block current through the pore more effectively compared to clusters farther away from the constriction region.<sup>72</sup> So if the cluster is in this orientation near the constriction ring, it will show a greater reduction in the cluster-induced current blockade and scale with the analyte residence time enhancement.

Figure 13 shows that the PEG mean residence times averaged over a wide range of different PEG sizes at 70 mV applied voltage increase in conjunction with an increase in the cluster-induced blockade. This particular set of data shows four distinct orientations of the cluster corresponding to different cluster state currents (Figure 13, inset), each centered at  $\langle i_{0,g} \rangle = -171.0$  pA,  $-169.1$  pA,  $-166.8$  pA, and  $-164.7$  pA. The left-most peak corresponds to a cluster position and orientation that comparatively does not block as much current ( $\langle i_{0,g} \rangle = -171.0$  pA), and results in lower residence times across all PEG sizes. In contrast, the right-most peak indicates a position and orientation that is closer to the constriction ring, blocking more ionic current flow ( $\langle i_{0,g} \rangle = -164.7$  pA), and corresponding to longer-lived PEG events.

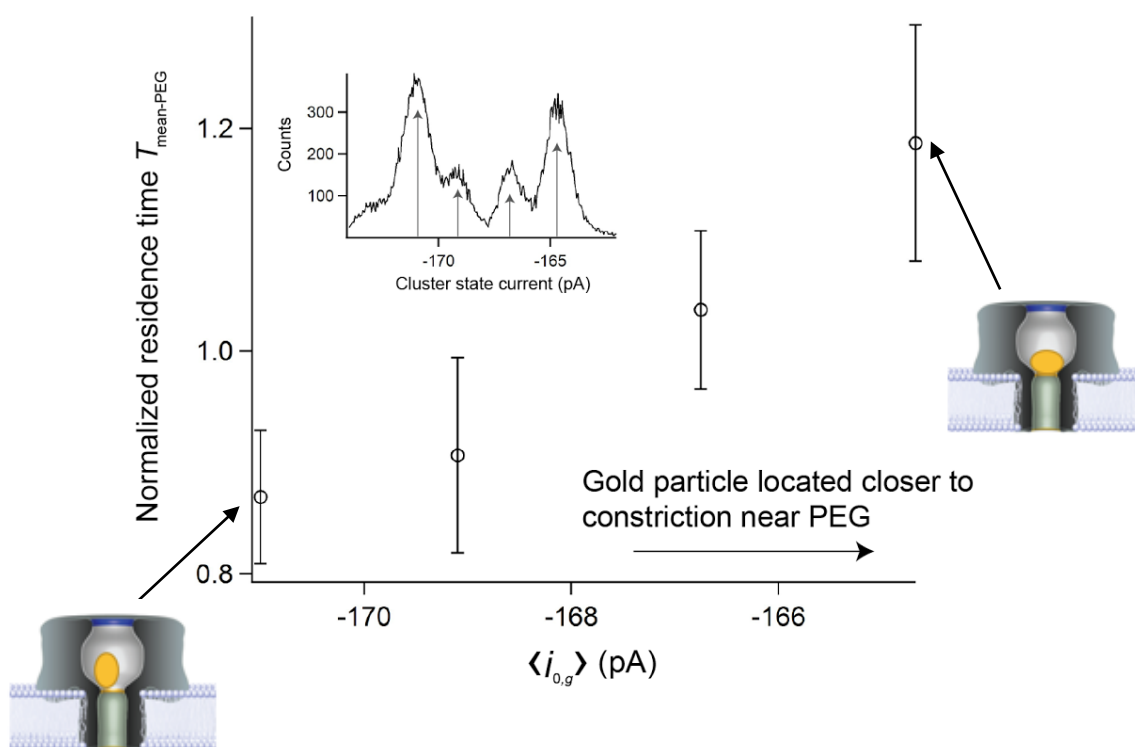


**Figure 13:** PEG residence times increase as the cluster is oriented closer to the constriction ring and positioned deeper into the nanopore. **(Inset)** A sample distribution of four distinct cluster-induced blockade states. All error bars correspond to  $\pm 1$  S.D.<sup>69</sup>

### 3.1.3.1. Normalizing residence times over a wide range of PEG sizes

In order to quantify the dependence between the gold cluster states and PEG residence times over a wide range of PEG sizes (Figure 13, y-axis), the mean residence time for a given PEG size ( $n$ -mer) must be normalized by the average mean residence time from all four cluster-states. The following formula is used to quantify the global mean PEG residence time over this wide range.

$$T_{mean-PEG} = \frac{\sum_{n=n_i}^{n_f} \frac{\langle \tau_{n,p} \rangle}{A_n}}{N} \quad (1)$$

Where  $\langle \tau_{n,p} \rangle$  is the mean residence time for a given  $n$ -mer PEG ( $PEG_n$ ) measured from cluster blockade state  $p$ . The sum is then calculated over a set of  $N$  PEG sizes ranging from  $n_i$  to  $n_f$  and normalized using  $A_n$  which is given by,

$$A_n = \frac{\sum_{p=1}^P \langle \tau_{n,p} \rangle}{P} \quad (2)$$

where  $P$  is the total number of gold cluster states (Figure 13, inset shows  $P = 4$ ). Taking the average over a wide range of PEG sizes using equations (1) and (2) indicates that PEG events from larger magnitude cluster blockade states exhibit greater residence time enhancement. The interaction between PEG and the cluster is clearly a crucial component of analyte residence time enhancement.

### 3.1.3.2. Optimizing the voltage for cluster-based residence time enhancement

Figure 14 shows how 60 mV, the ideal transmembrane potential, is connected to cluster position. The distribution of  $PEG_{28}$  residence times at 50 mV, 60 mV, and 70 mV in terms of cluster blockade display the cluster's behavior with varying voltages. The cluster will block between 15%-30% of the ionic current through the pore. 50 mV is not strong enough to push the cluster into position on top of the constriction ring, and cannot yield the longer residence times the

system is capable of producing. 70 mV is too large of a transmembrane voltage because the clusters are more likely to occupy various orientations and positions within the nanopore, indicated by the spread of different data points. 60 mV yields a more uniform distribution of cluster states within the pore. At this voltage the cluster is more closely localized to the constriction ring and this allows for stronger interactions with PEG molecules.

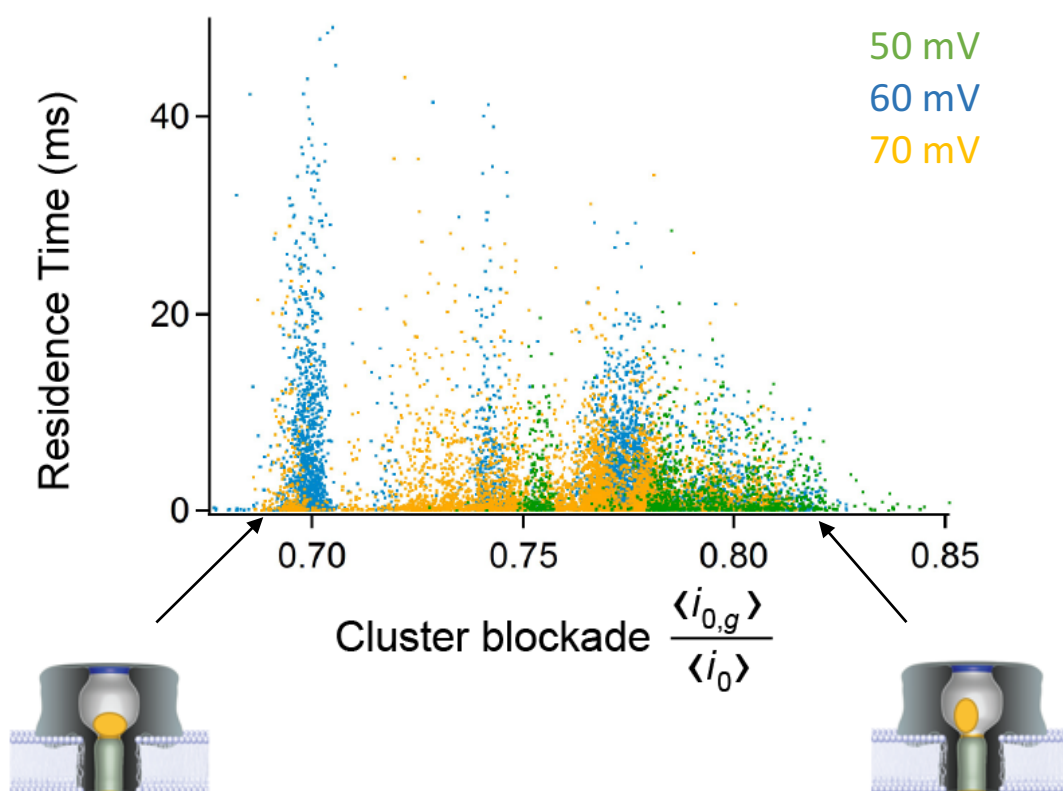


**Figure 14:** The distribution of residence times at 50 mV (green), 60 mV (blue) and 70 mV (gold) for the gold occupied pore compared to the degree of the cluster blockade. Figures show an approximate orientation of the cluster within the pore in terms of a cluster blockade state. This data was recorded using 10  $\mu\text{M}$  PEG<sub>28</sub>.<sup>69</sup>

### 3.1.4. PEG on-rate

Theoretically, for a bulk PEG concentration of 1  $\mu\text{M}$ , the PEG on-rate to  $\alpha\text{HL}$  should be around 1000 events per second via the Smoluchowski equation.<sup>56</sup> However, a number of articles have noted a lower than expected on-rate for the analyte concentration studied.<sup>67,70,71,73</sup> Additionally, the on-rate for cationic PEG should increase with increasing transmembrane potential.<sup>25,28</sup> However, the opposite occurs as shown in Figure 15 (black circles) where the observed on-rate of PEG<sub>28</sub> decreases. These results are most likely due to many collisions between PEG and the pore going undetected at typical bandwidths used for nanopore sensing.<sup>74,75</sup> Our sensing platform (Section 2.3.4.) has a bandwidth of 10 kHz, so that the cutoff time for detecting a blockade event is 100  $\mu\text{s}$ . If a PEG molecule resides in the pore for less than 100  $\mu\text{s}$ , its blockade event will go undetected (Figure 16). Therefore, using metallic clusters to increase the PEG-pore interaction time should increase the observed hit-rate of PEG with the pore. (Figure 15, red curve).

#### 3.1.4.1. Using a correction factor $k_c$

A gold cluster increases PEG's residence time within the nanopore, overall increasing the observed PEG on-rate. Figure 14 shows that the on-rate of PEG<sub>28</sub> increases when a cluster is present in the pore. To verify that this observation is caused by missing events, we correct the observed hit rate,  $k_{\text{obs}}$ , by including a factor that accounts for events that are too short to be detected by our system. The corrected hit rate of PEG to pore,  $k_c$ , follows from noting that the PEG residence time distribution is well described by a single exponential function (Figure 16).

$$k_c = \frac{k_{\text{obs}}}{\int_{t_{\text{cut}}}^{\infty} \frac{e^{(-t/\tau)}}{\tau} dt} = k_{\text{obs}} e^{(t_{\text{cut}}/\tau)} \quad (3)$$

where  $\tau$  is the PEG mean residence time, and  $t_{cut}$  is the cutoff time for detecting a blockade ( $t_{cut} = 100 \mu\text{s}$ ). The corrected on-rate appears to agree with the observed on-rate in the gold occupied state, indicating that the gold-based residence time enhancement has the added benefit of yielding a more accurate estimate of the on-rate of PEG to the pore.

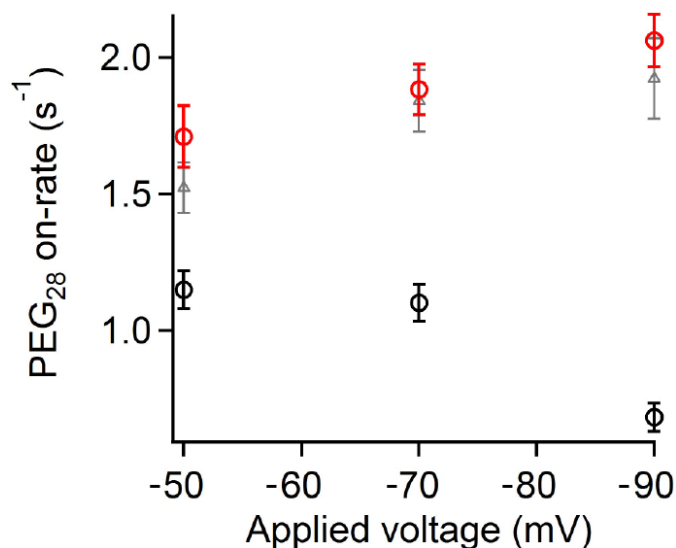


**Figure 15:** The PEG<sub>28</sub> on-rate kinetics are more effectively measured with gold present in the pore (red circles). If gold is absent, the PEG<sub>28</sub> on-rate is reduced with increasing applied voltage (black circles). Events that are too short to be detected can be approximated in this figure using a correction factor,  $k_c$ , applied to the black data points. This data was recorded using 5 $\mu$ M PEG<sub>28</sub>. Error bars correspond to  $\pm 1$  S.D.<sup>69</sup>

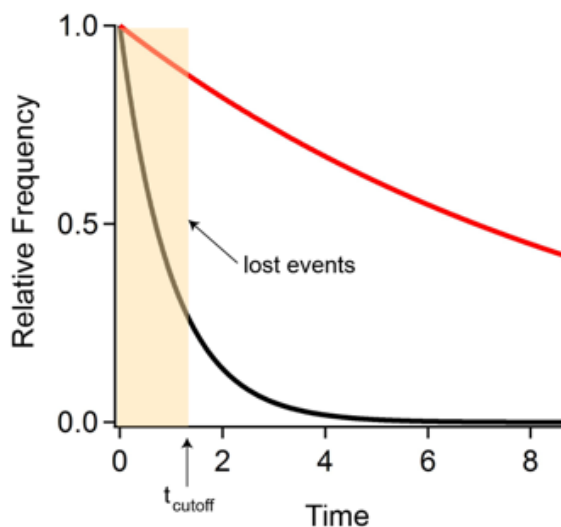


**Figure 16:** PEG on-rate to a nanopore is well described by a single exponential function. Many events are lost without a gold cluster in the nanopore (black curve). Incorporating a gold cluster lengthens PEG residence time allowing for more blockade events to be detected (red curve).<sup>69</sup>

### 3.2. Expanding beyond PEG sensing

In order to demonstrate the broader applicability of nanopore spectrometry, it is necessary to move beyond PEG molecules. The first goal is to simply demonstrate that nanopore spectrometry can be used for any polymer besides PEG. Another common polymer, Poly-L-Lysine, with several molecular weights (Figure 17), a helical structure, and extremely cationic at a neutral pH<sup>76</sup> was analyzed using the SMNS method. For simplicity the difference in charge between PEG and PLL will be neglected and this section will only compare differences in current blockade depth corresponding to molecule size. As seen with PEG, PLL exhibited a similar comb-like peak distribution (Figure 18 A,B). Compared to the PEG distribution, the PLL blockade peaks showed wider spacing between each peak. Plotting arbitrarily assigned peak numbers and their blockade depth yields a linear relationship (Figure 18 C). By taking the least-squares fit of this data we obtain a slope of  $69.0 \pm 0.2$  for PEG and  $29.7 \pm 0.3$  for PLL. To show that we can correlate the spacing between PLL blockade peaks and the mass of individual PLL monomer units, the ratio between the molecular weight monomer units of each molecule will match the ratio of these two slopes. The ratio between these two slopes is  $m_{\text{PEG}}/m_{\text{PLL}} = 2.3 \pm 0.02$  and is in qualitative agreement with the ratio between the two monomer units ( $128n/44n = 2.9$ ) this supports the notion that SMNS may be a viable tool to predict the mass of unknown analyte.

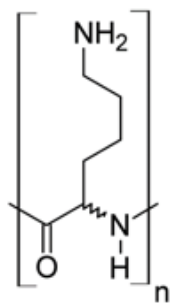


**Figure 17:** Structure of PLL where  $n$  indicates the degree of polymerization.  $MW_{\text{PLL}} = (128 \text{ g/mol})n$  (<http://www.sigmaaldrich.com>).

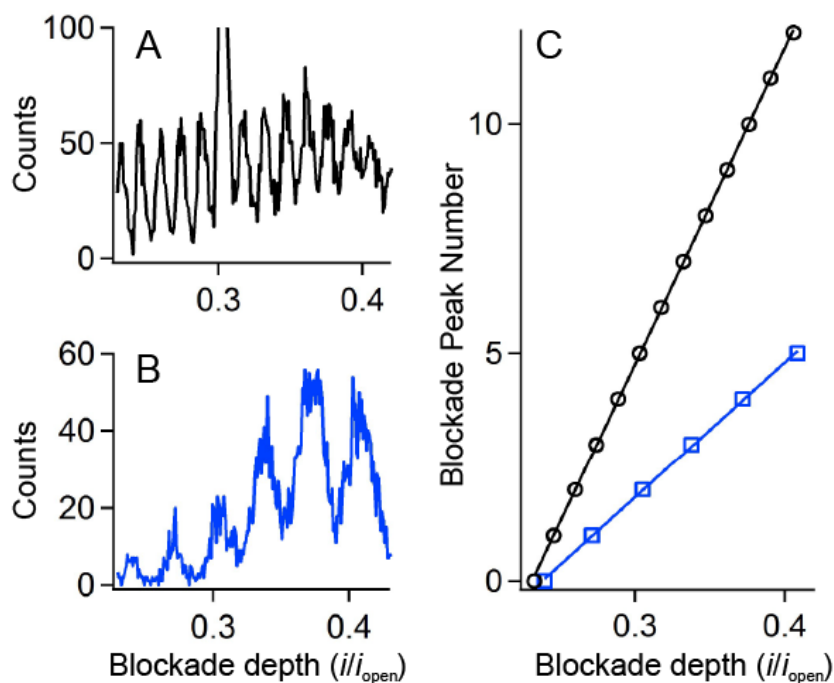


**Figure 18:** SMNS correctly predicts the relative difference of PEG and PLL monomer molecular weights. **(A)** The current blockade distribution of PEG. **(B)** A similar comb-like distribution for PLL. **(C)** Plotting arbitrary peak numbers vs. blockade depth for PEG (black) and PLL (blue) yields slopes of  $69.0 \pm 0.2$  (PEG) and  $29.7 \pm 0.3$  (PLL).

**Table 2:** Peptides chosen for this study arranged in increasing size.

Peptide	Amino Acid Sequence	Mol wt (g/mol)
leu-enkephalen	Tyr-Gly-Gly-Phe-Leu	555.62
angiotensin II	Asp-Arg-Val-Tyr-Ile-His-Pro-Phe	1046.18
angiotensin I	Asp-Arg-Val-Tyr-Ile-His-Pro-Phe-His-Leu	1296.48
QBP1	Ser-Asn-Trp-Lys-Trp-Trp-Pro-Gly-Ile-Phe-Asp	1435.58
neurotensin	Gly-Leu-Tyr-Glu-Asn-Lys-Pro-Arg-Arg-Pro-Tyr-Ile-Leu	1672.92

### 3.3. Using SMNS for peptide detection

Motivated by the initial results with PLL, a variety of water-soluble, near-neutral peptides (Table 2) were analyzed using single molecule nanopore spectrometry. Each peptide gave rise to well-defined, unimodal blockade peaks that were distributed consistently according to their size (Figure 19A). The deepest current blockade peak corresponds to the largest peptide, neurotensin, and the shallowest blockade corresponds to the smallest peptide, leu-enkephalen. These results are consistent with the blockade distribution correlation to molecular size found with PEG in which the larger PEG monomer units exhibited deeper current blockades.<sup>25</sup> Additionally, the residence times of each peptide were investigated and yielded single exponential distributions (Figure 19B). With the exception of QBP1, our results showed longer mean residence times for larger peptides and shorter mean residence times for smaller peptides. The largest peptide neurotensin has a mean residence time  $\tau_{\text{neuro}} = (6.7 \pm 0.2)$  ms and the smallest peptide leu-enkephalen,  $\tau_{\text{leu-e}} = (0.016 \pm 0.001)$  ms. Previous results using PEG showed a similar trend where larger molecules would consistently yield longer residence times within the nanopore, further indicating that the SMNS method is a powerful tool that can be used for peptide analysis.

#### 3.3.1. Debye screening length

The debye length for a 1:1 electrolyte of concentration 3M is calculated using,

$$\kappa^{-1}(nm) = \frac{0.304}{\sqrt{I(M)}}$$

and is found to be  $\kappa^{-1} = 0.176nm$ .<sup>77</sup> The diameter of the inner lumen of the nanopore is much larger than this (see Section 1.1.2.), therefore the majority of any peptide-pore Coulombic interactions can be essentially ignored.

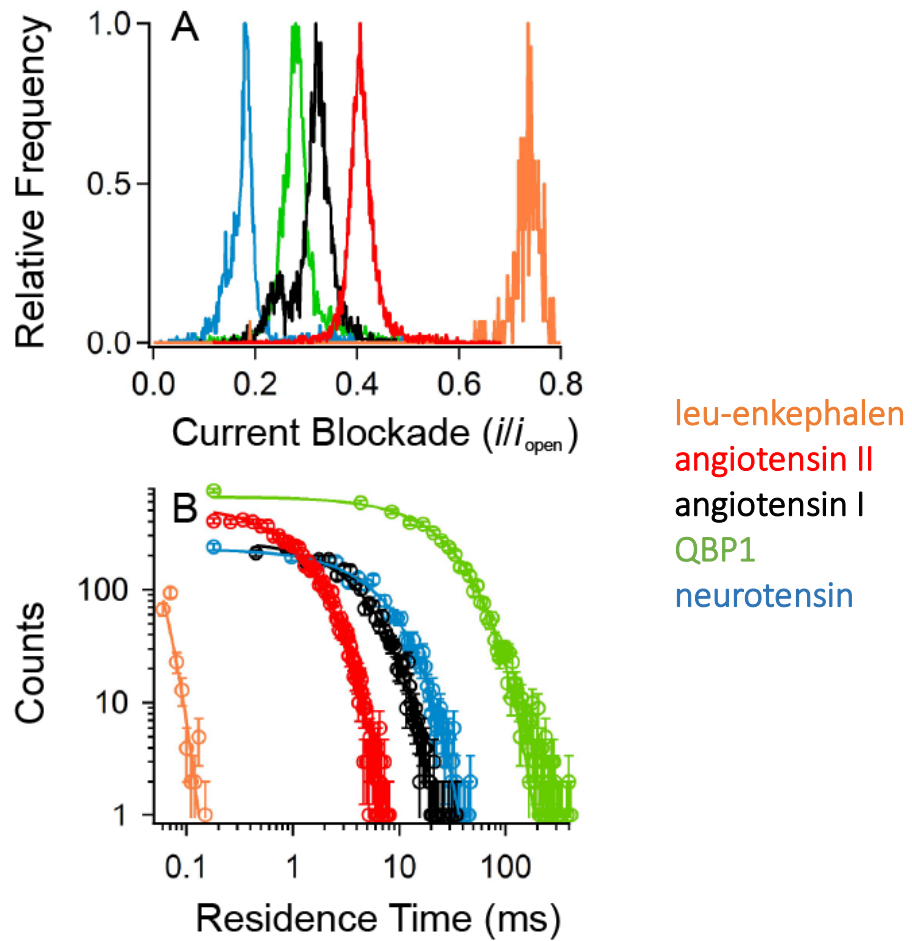


**Figure 19:** SMNS for peptide detection. **(A)** Current blockade distributions for all five peptides. **(B)** Residence time distributions for all five peptides.

### 3.3.2. Peptide correlation with PEG

Figure 20 shows the relationship between current blockade depth and the molecular weight of polydisperse PEG (black circles) mixture and the aforementioned peptides (solid squares). The agreement between the PEG and peptide data suggests the ability to assign molecular weights based on the magnitude of current blockades. A theoretical model discussing the connection between current blockade ratio and molecular will be presented later in the thesis (see Section 4.2).

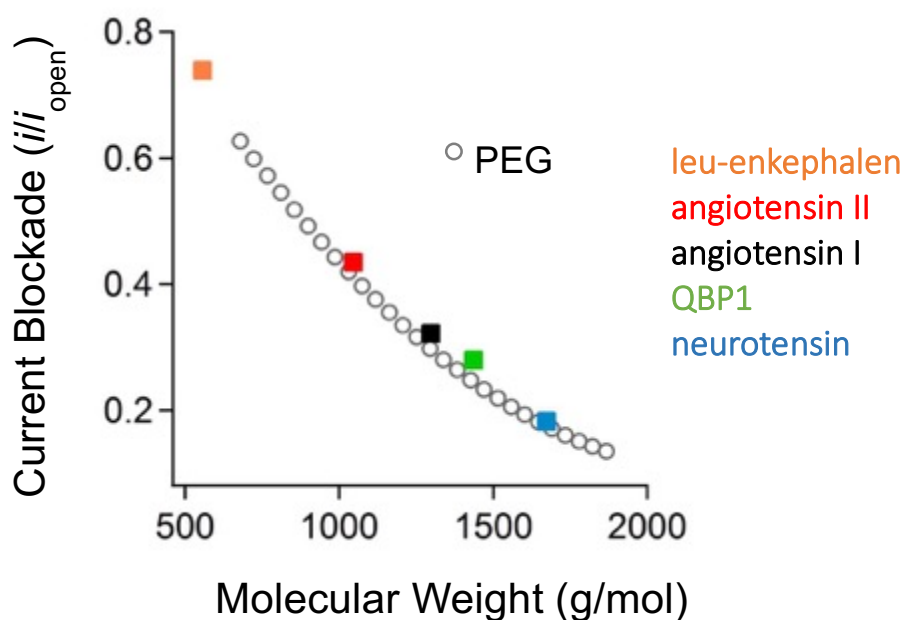


**Figure 20:** A distribution of current blockade peaks and their corresponding molecular weight for PEG (open circles) and peptides (squares).

### 3.3.3. Peptide enhancement using Au<sub>25</sub>(SG)<sub>18</sub>

Section 1.2.1.1. discussed previous work where a single gold cluster in the pore greatly improves the SMNS sensing capabilities of the pore.<sup>57</sup> This earlier work showed that when a charged cluster is present within the *cis*-side region of a nanopore, a PEG molecule entering the *trans*-side will have over an order of magnitude increased residence time in addition to an increased on-rate to the pore. This increased the resolution of current blockade distributions using SMNS analysis. Motivated by this enhancement, the role that gold clusters may play in enhancing peptide detection was investigated. The current blockade peaks of three largest/cationic peptides, angiotensin I, angiotensin II, and neurotensin, are analyzed in an empty pore versus a gold-occupied pore (Figure 21 A-C). The quality of these current blockades will partially depend on the mean residence time of the peptide within the pore. In a gold cluster-occupied nanopore, peptides not only demonstrated similar improvements in mean residence time, but also improvements in the observed peptide on-rate to the nanopore (Table 3).

**Table 3:** The on-rate ( $k_{\text{on}}$ ) and residence time ( $t_{\text{res}}$ ) of each peptide improves in a gold-occupied pore.

Peptide		Empty pore	Gold-occupied pore
angiotensin II	$k_{\text{on}}$	2.27 s <sup>-1</sup>	2.76 s <sup>-1</sup>
	$t_{\text{res}}$	1.15 ms	2.06 ms
angiotensin I	$k_{\text{on}}$	3.33 s <sup>-1</sup>	4.08 s <sup>-1</sup>
	$t_{\text{res}}$	3.85 ms	12.0 ms
neurotensin	$k_{\text{on}}$	2.66 s <sup>-1</sup>	5.06 s <sup>-1</sup>
	$t_{\text{res}}$	8.05 ms	21.9 ms

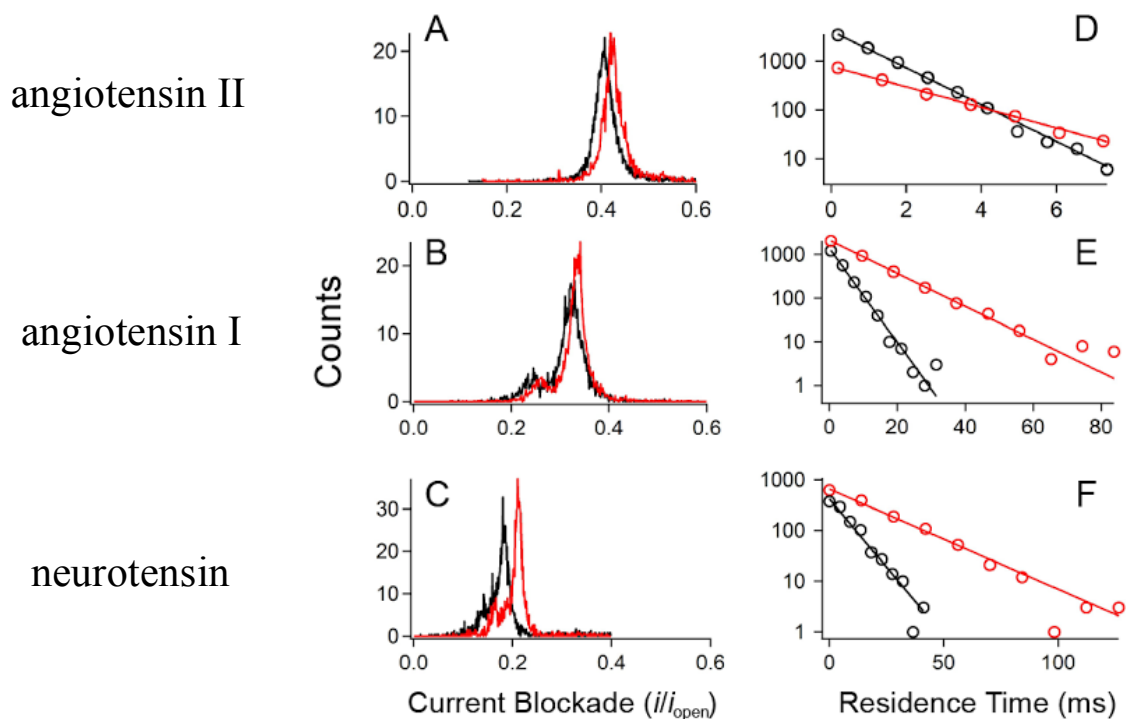


**Figure 21:** Gold clusters enhance current blockade and residence time distributions for each peptide, (A, D) angiotensin II. (B, E) angiotensin I. (C, F) neurotensin.

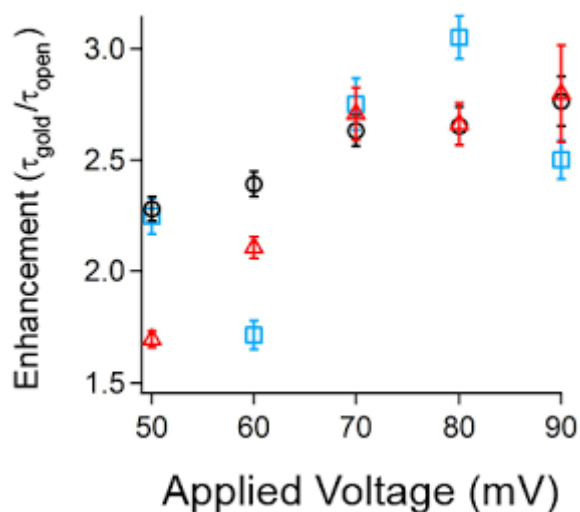


**Figure 22:** The cluster-induced enhancement improves with increasing voltage for angiotensin I (black circle), angiotensin II (red triangle), and neurotensin (blue square).

The Coulombic interaction between the oppositely charged gold cluster and peptide plays an important role in increasing the mean residence time of a peptide within the nanopore. As seen previously with PEG (Section 3.1.1.), the peptide residence time will increase with increasing transmembrane potential. The applied electric field forces the peptide and cluster to interact more strongly within the pore volume. Figure 22 shows how the enhancement ratio of each peptide with and without a gold cluster in the pore ( $\tau_{\text{gold}}/\tau_{\text{open}}$ ) grows with increasing voltage.

### **3.3.4. Altering solution conditions**

The degree of noise within individual blockades has shown to be greater using peptides, than previously studied PEG molecules (Figure 23B). Noise can be parameterized using the standard deviation of each blockade (Figure 23A), so to further improve the resolution of current blockade peaks it is necessary to decrease the standard deviation of each blockade. Peptides have a more complicated secondary structure, which may be indicated by this degree of noise. By adjusting solution conditions, like decreasing pH and adding a denaturing agent, the charge, and therefore, the structure of a peptide can be changed (Figure 24). This will not only enhance the charge-charge interaction between the peptide and cluster, but will also decrease the standard deviation of a peptide's current blockade.

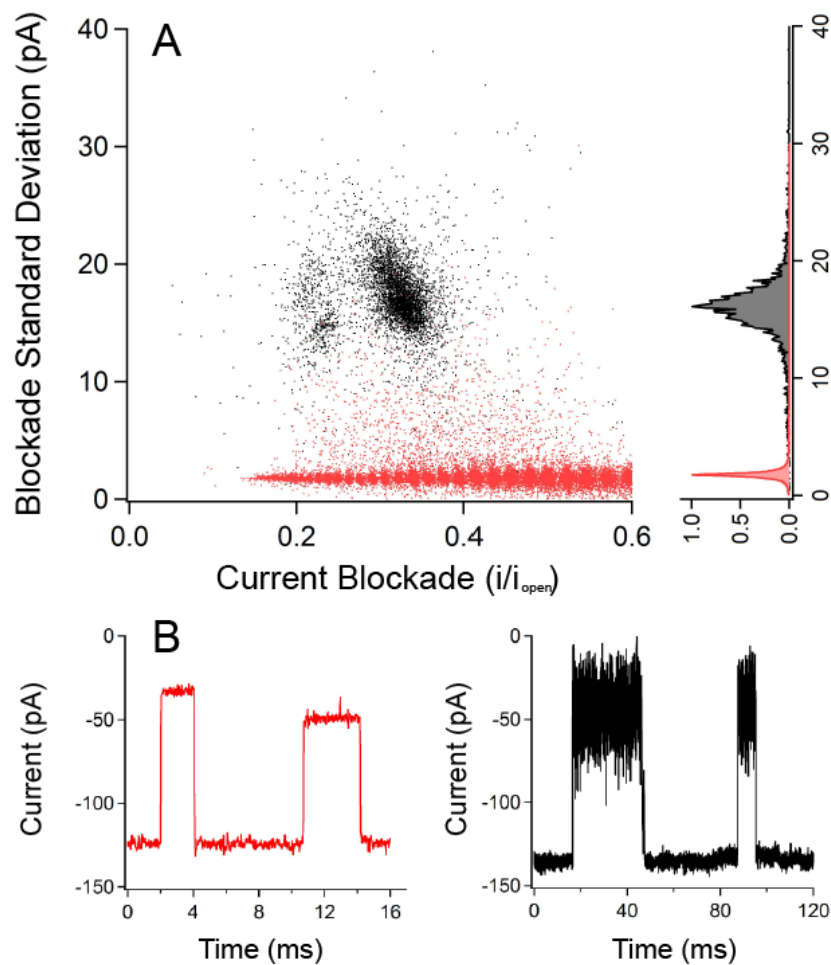


**Figure 23:** Noise and standard deviation comparisons between the current blockades for PEG (red) and angiotensin I (black). **(A)** Peptide blockades exhibit a larger standard deviation resulting from **(B)** a greater degree of noise in a given blockade. This is expected given the more complicated secondary structure expected for these peptides.

### 3.3.4.1. Adjusting solution pH

As shown in section 3.3.3., there is a Coulombic interaction between the peptide and gold cluster that enhances the residence time of a peptide within the pore. By lowering the pH of an electrolyte solution, the charge of a peptide like can be increased (Figure 24). This will increase the interaction between the cluster and peptide, leading to an increased mean residence time for that peptide. Additionally, increasing the charge may change the peptide's structure in a way that decreases each blockade's standard deviation (Figure 23A). Lowering the standard deviation and increasing the mean residence time improves the selectivity of the pore by providing more accurate estimates of the mean blockade current.<sup>57</sup>

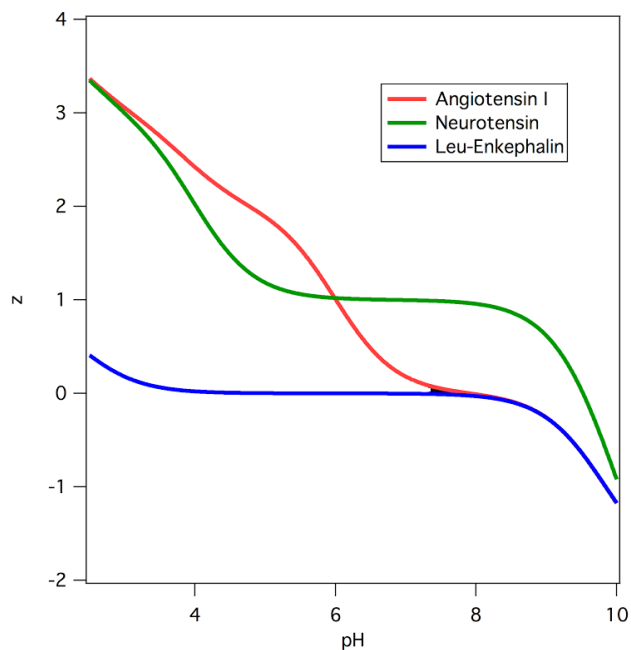


**Figure 24:** By lowering the solution pH, the net charge of a peptide can be increased. (Image created by Joseph W.F. Robertson (NIST, Gaithersburg, MD) using Proteochem)

Parameterizing the observed enhancement using,

$$\gamma = \frac{(\tau_{off})^{1/2}}{S.D.} \quad (3)$$

shows that lowering the pH will improve the sensing capabilities of the pore. By decreasing the electrolyte solution pH to 5.8, the charge of Angiotensin I increases to  $z = 1.2e$  (Figure 24), which lowered the standard deviation (Figure 25A), increased the mean residence time, and improved the observed enhancement (Figure 25B).

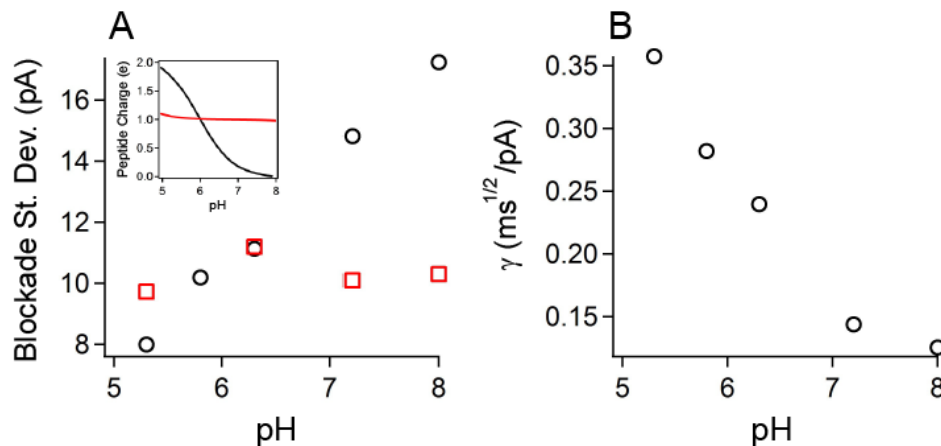


**Figure 25:** pH of solutions is correlated to blockade fluctuations (**A, inset**) Estimated peptide charge according to pH of solution. (**A**) The mean standard deviation of current blockades for angiotensin I (black circles) and neurotensin (red squares) with varying solution pH. (**B**) The enhancement factor with varying solution pH. Larger values for the enhancement factor  $\gamma$  correlate with narrower peaks in current blockade distributions. These narrower peaks allow for a more accurate connection between a given blockade and a particular peptide.

### 3.3.4.2. Adding a denaturing agent

Residence time has proven to be a critical component towards improving the resolution of a current blockade peak. However, this sensing technique can only improve peak resolution by a finite amount. Lowering the pH of an electrolyte solution has shown to increase the charge, thereby altering the structure of a peptide in a way that reduces the standard deviation of current blockades. The final step in optimizing angiotensin I detection using SMNS was to take this structural change further by introducing a denaturing agent, guanidinium hydrochloride (Gdm-HCl). Gdm-HCl caused a reduction in the mean standard deviation of each event (Figure 26C(iv)) which further improved the resolution of the angiotensin I current blockade peak (Figure 26A(iv)).

### 3.3.5. Optimizing peptide detection

The degree of optimization previously achieved using PEG (B, blue line) should also be possible in peptide sensing. Figure 26 shows how each step in the optimization process affects the full width at half maximum (FWHM) of angiotensin I's current blockade peak. A(i) displays an angiotensin I current blockade peak with no adjustments, in a pH 7.2 solution. By changing the solution conditions to pH 5.8, the residence time ( $t_{\text{off}}$ ) increased and standard deviation (S.D.) decreased (C(ii)) resulting in a more resolved current blockade peak (A(ii)). As seen before, the inclusion of a gold cluster further improves the FWHM by increasing the residence time of angiotensin I in the nanopore (A(iii)). Finally, incorporating the denaturing agent, Gdm-HCl, decreased the standard deviation, so that the final current blockade peak has a FWHM similar to optimized PEG results (A(iv)). Part B displays each step in the peptide optimization process narrows the width of each blockade peak, showing that SMNS is capable of detecting peptides with the same level of sensitivity as PEG.

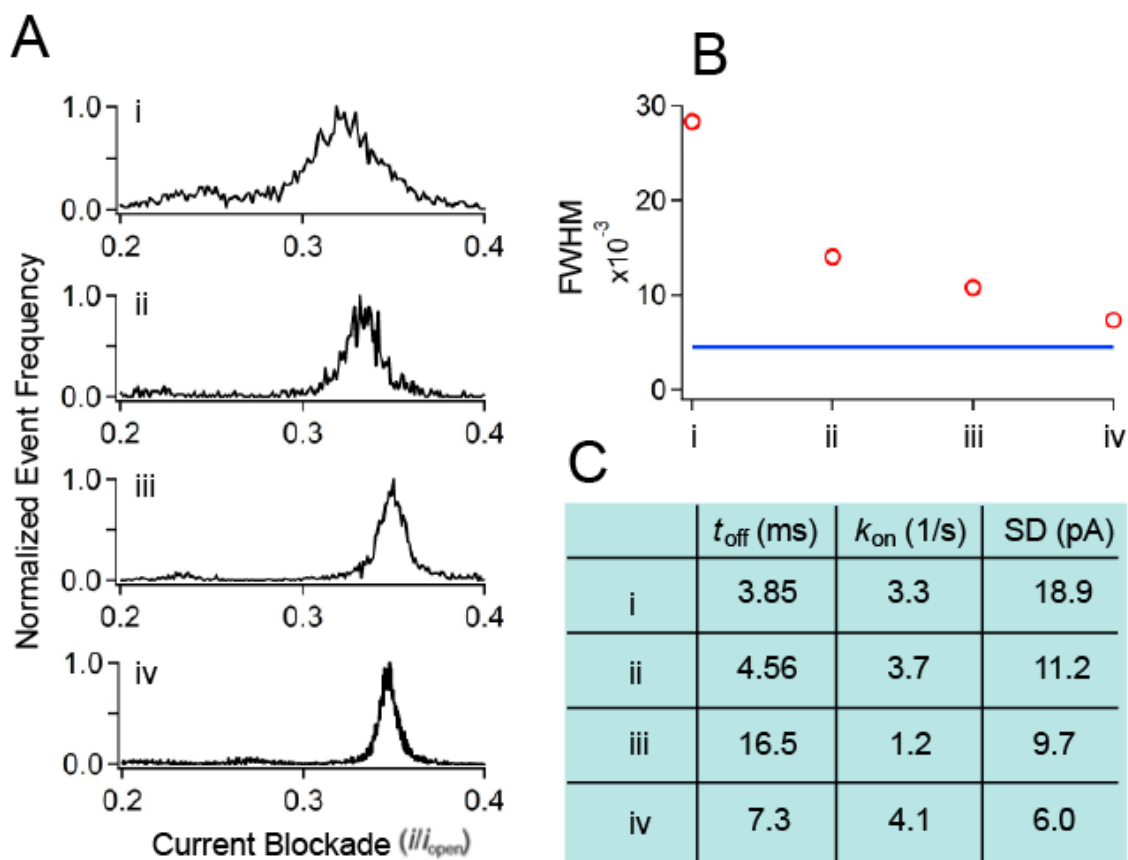


**Figure 26:** Optimizing peptide detection using SMNS. **(A)** angiotensin I's current blockade peak improves with system adjustment. (i) pH 7.2, (ii) pH 5.8, (iii) pH 5.8 and a gold cluster in the pore, (iv) pH 5.8, 1M Gdm-HCl, and a gold cluster in the pore. **(B)** The width of each blockade peak (FWHM) decreases with each level of enhancement (i-iv), showing that peptide detection is capable of the same level of sensitivity as seen with PEG (blue line). **(C)** Mean residence time ( $t_{off}$ ), on-rate ( $k_{on}$ ), and standard deviation (S.D.) of angiotensin I with each system adjustment (i-iv).

## 4. DISCUSSION

### 4.1. Understanding Au<sub>25</sub>(SG)<sub>18</sub> PEG enhancement

When a gold cluster enters a nanopore, the voltage profile of a pore is modified leading to a reduction in the applied electric field. This could be one explanation for the increased residence time of PEG. However, a decrease in the electric field generally results in a reduction of the PEG on-rate to the pore.<sup>28</sup> This contradicts results shown in Figure 15 where PEG<sub>28</sub>'s on-rate increased with a gold cluster present in the nanopore. As hypothesized earlier, there must be some interaction between PEG and the cluster that gives these results.<sup>57,69</sup>

#### 4.1.1. Current blockade distribution shift

Figure 8 shows a rightward-shift in the current blockade distribution when a cluster enters the pore. In order to understand this shift, an expression describing the ratio of the current blockade peak positions with and without a gold cluster in the pore must be derived. The nanopore sensor can be modeled as a series of Ohmic resistors (with linear I-V dependence) as shown in Figure 27. As discussed in Section 1.1.2. the  $\alpha$ -hemolysin pore structure consists of a large *cis*-side vestibule and a narrow *trans*-side lumen.<sup>8</sup> The total resistance of the nanopore can then be described as a series of two resistors,

$$R_{total} = R_{trans} + R_{cis}$$

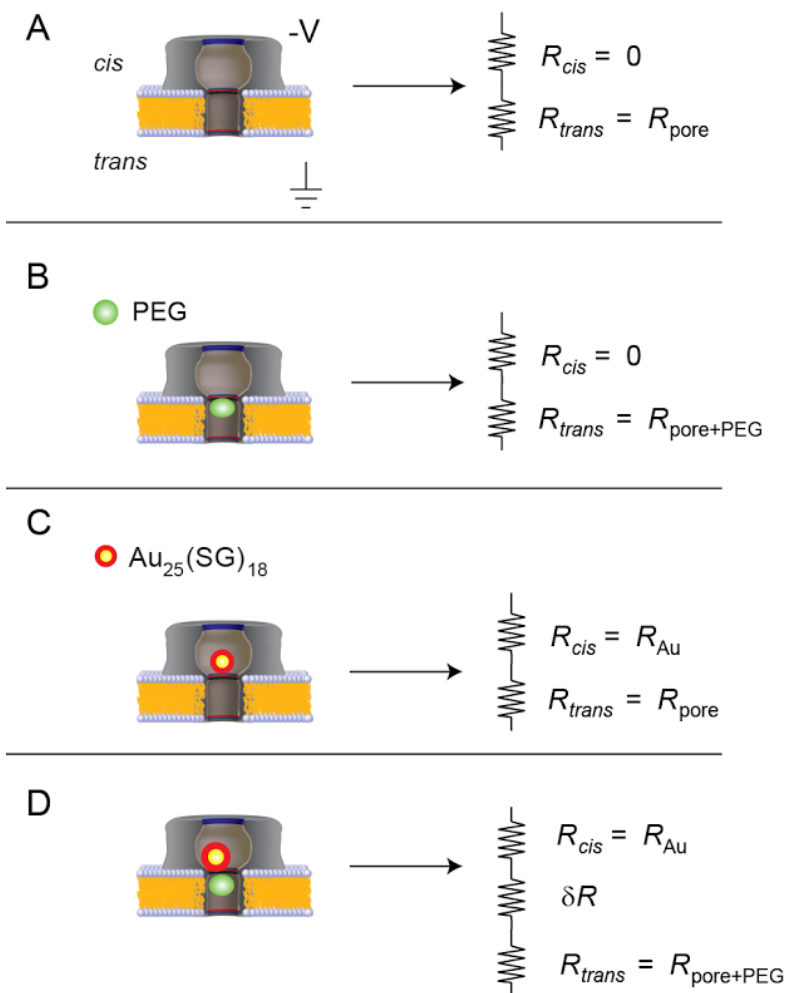


**Figure 27:** Schematic illustration of the ohmic model of an  $\alpha$ -hemolysin nanopore. One of four possible configurations of the nanopore occur when  $Au_{25}(SG)_{18}$  is on the *cis*-side of the nanopore and PEG is on the *trans*-side. **(A)** Open pore configuration. **(B)** PEG in the *trans*-side of the nanopore. **(C)**  $Au_{25}(SG)_{18}$  in the *cis*-side of the nanopore. **(D)** PEG and  $Au_{25}(SG)_{18}$  both in the nanopore.<sup>69</sup>

The access resistance of the gold cluster entering the pore is being neglected due to its small size and rapid entrance time relative to our bandwidth and sampling frequency. If the pore is empty, the resistance will be dominated by the *trans*-side lumen<sup>78</sup> and can be defined as,

$$R_{trans} = R_{pore}$$

$$R_{cis} = 0$$

If a PEG molecule enters the *trans*-side, the resistance on the *trans*-side will increase to,

$$R_{trans} = R_{pore+PEG}$$

If a cluster enters the *cis*-side, the resistance on the *cis*-side will increase to,

$$R_{cis} = R_{Au}$$

So that the total resistance of the nanopore can then be described as,

$$R_{total} = R_{pore+PEG} + R_{Au} + \delta R$$

where  $\delta R$  indicates a change in resistance due to any structural changes from the interaction between PEG and gold, possibly causing this shift in peak position. In order to verify this claim, the time-averaged open pore current ( $\langle i_0 \rangle$ ) under an applied transmembrane voltage ( $V$ ) is described using Ohm's law,

$$\langle i_0 \rangle = \frac{V}{R_{pore}} \quad (4)$$

The time-averaged current when only a gold cluster is in the pore,

$$\langle i_{0,g} \rangle = \frac{V}{R_{pore} + R_{Au}} \quad (5)$$

The time-averaged current when only PEG<sub>n</sub> is in the pore,

$$\langle i \rangle = \frac{V}{R_{pore+PEG_n}} \quad (6)$$

and the time-averaged current when both PEG<sub>n</sub> and Au are in the pore,

$$\langle i_g \rangle = \frac{V}{R_{Au} + R_{pore+PEG_n} + \delta R} \quad (7)$$

The relative shift in the peak positions once the cluster enters the nanopore is defined by,

$$S_n = \frac{[\langle i_g \rangle / \langle i_{0,g} \rangle]_n}{[\langle i \rangle / \langle i_0 \rangle]_n} \quad (8)$$

where  $n$  refers to the polymer repeat number for a given peak in the current blockade distribution.

Substituting equations (4) - (7) into equation (8) yields,

$$S_n = \left( \frac{R_{pore} + R_{Au}}{R_{Au} + R_{pore+PEG_n} + \delta R} \right) \left( \frac{R_{pore+PEG_n}}{R_{pore}} \right) \quad (9)$$

In order to further simplify this, an expression ( $b_n$ ) indicating the position of the  $n^{\text{th}}$  peak in an open pore will be derived. This is the PEG<sub>n</sub>-induced current blockade ratio with no gold present and can be calculated by dividing equation (6) by equation (4).

$$b_n = \left[ \frac{\langle i \rangle}{\langle i_0 \rangle} \right]_n = \frac{R_{pore}}{R_{pore+PEG_n}} \quad (10)$$

A second expression ( $c$ ) describing the ratio of the open pore current and the current with a gold cluster in the pore can be derived by dividing equation (4) by equation (5).

$$c = \frac{\langle i_0 \rangle}{\langle i_{0,g} \rangle} = \frac{R_{pore} + R_{Au}}{R_{pore}} \quad (11)$$

Expressions  $b_n$  and  $c$  are then be substituted in equation (9) and manipulated to obtain a simpler expression for  $S_n$ ,

$$S_n = \frac{c}{1 - b_n(1 - c) + d(V)} \quad (12)$$

where,

$$d = \frac{\delta R}{R_{pore+PEG_n}}$$

and is the relative change in the resistance due to the interaction between PEG and the cluster. This parameter depends on the applied voltage  $V$  and the size of the  $PEG_n$  molecule; however, to minimize the number of free parameters in the model,  $d$  is assumed to be a constant.

#### 4.1.2. PEG/cluster structural change

The interaction between PEG and the cluster most likely result in structural changes to either the PEG and/or cluster. Figure 28 shows the shift in the current blockade distribution by examining measured values of  $S_n$  (equation (12)) over a range of applied voltages. First, it should be observed that  $d$ , the interaction strength, scales linearly with the applied voltage (Figure 28, inset) which is consistent with the resident time-mechanism hypothesis. If there is no interaction

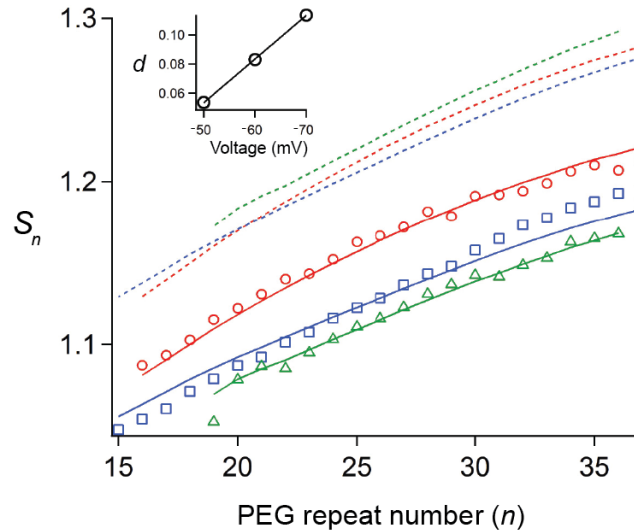


**Figure 28:** The current blockade distribution of experimental data (open symbols) with least-squares fitting, and the distribution when  $d = 0$  using equation (12) (dashed lines). There is a linear relationship between  $d$  and applied voltage (inset). (red = 50mV, blue = 60mV, green = 70mV)<sup>69</sup>

term or structural change (i.e.  $d = 0$ ), then we would observe a larger shift in  $S_n$  (Figure 28, dashed lines). However, we observed a smaller shift (Figure 28, open symbols). The interaction term  $d$  serves to reduce the magnitude of the peak shifts thus verifying that  $d$  is nonzero; and that there is most likely a structural change in either PEG and/or the cluster upon interaction within the pore.

#### 4.1.3. $K^+$ interaction with PEG

Section 3.1.3. discussed how the oppositely charged PEG and cluster are attracted to each other when located closer to the constriction region of the pore. This Coulombic attraction is dependent on the charge of PEG. Previous studies show that neutral PEG molecules become charged because they to bind  $K^+$  in high ionic strength conditions.<sup>25,28</sup> One way to test the validity of our peak shift model (Figure 28) is to conduct a study where PEG is not charged when it interacts with the cluster inside the pore. A previous study suggests that lithium cations will not bind to PEG,<sup>70</sup> and therefore, in a high ionic strength LiCl solution, PEG should remain neutral. This will be verified if the interaction term  $d$  in LiCl ( $d_{LiCl}$ ) is less than the interaction term in KCl ( $d_{KCl}$ ).

The current blockade shifts for PEG<sub>28</sub> using LiCl and KCl were compared. Using LiCl, PEG<sub>28</sub> had a mean normalized current blockade when a cluster was present,

$$\left[ \frac{\langle i_g \rangle}{\langle i_{0,g} \rangle} \right]_{n=28} = 0.494$$

where  $\langle i_{0,g} \rangle = 57.0 \text{ pA}$ . The mean normalized current blockade without a cluster in the nanopore is,

$$\left[ \frac{\langle i \rangle}{\langle i_0 \rangle} \right]_{n=28} = 0.430$$

where  $\langle i_0 \rangle = 75.4 \text{ pA}$ . These two current blockades yield a blockade ratio  $S_{28} = 1.15$ . Applying these values to equation (12) leads to an interaction term,  $d_{LiCl} = 0.007$ . This is almost an order of

magnitude less than the interaction term for identical conditions in KCl,  $d_{\text{KCl}} = 0.054$ , and indicates that there is a stronger interaction between PEG and the cluster, and verifies that PEG is becoming more charged in a KCl solution by binding to  $\text{K}^+$ .

#### 4.2. Modeling the connection between analyte molecular weight and current blockade

Section 3.3.2. showed that PEG and peptides have a similar trend when plotting the mean blockade depth as a function of the peptide molecular weight. This agreement suggests the ability to assign molecular weights to unknown molecules based on the magnitude of their blockade depth. It is well established that PEG blockade peaks are separated at the single monomer unit. So to verify the universality of the relationship between analyte mass and current blockade depth, it is necessary to model the nanopore system (Figure 29) and estimate the connection between current blockades and corresponding analyte mass.

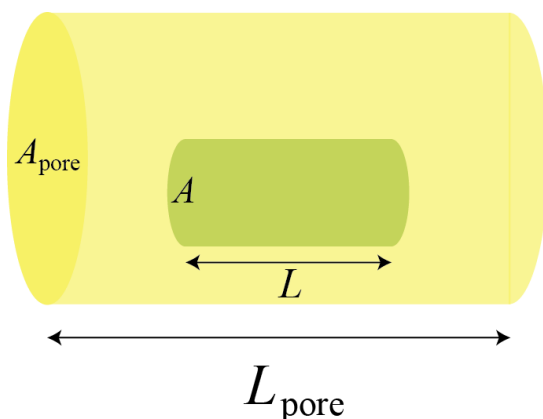


**Figure 29:** Molecular model of a nanopore with a molecule inside. The pore (yellow) is modeled as a cylinder with cross sectional area  $A_{\text{pore}}$  and length  $L_{\text{pore}}$ . A molecule (green) is also modeled as a cylinder with cross sectional area  $A$  and length  $L$ .

Following a similar approach as the model describing cluster-PEG interactions, we model the current blockade ratio as a ratio of two different resistances,<sup>28</sup>

$$\frac{\langle i \rangle}{\langle i_0 \rangle} = \frac{R_{open}}{R_{blocked}} = \frac{\frac{\rho_{open} L_{open}}{A_{open}}}{\frac{\rho_{open}(L_{open} - L)}{A_{open}} + \frac{\rho L}{A_{open} - A}} \quad (13)$$

where  $R_{open}$  is the open pore resistance and  $R_{blocked}$  is the resistance of the pore with a molecule inside the pore.

Resistance is then expanded in terms of the resistivity of the open pore,  $\rho_{open}$ , the resistivity of the pore within the vicinity of the molecule,  $\rho$ , the open pore length  $L_{open}$ , the molecule length,  $L$ , the open pore cross sectional area,  $A_{open}$ , and the the molecule cross sectional area,  $A$ . Minor manipulations rearrange equation (13) to,<sup>28</sup>

$$\frac{\langle i \rangle}{\langle i_0 \rangle} = \frac{1}{1 - \left(\frac{L}{L_{open}}\right) \left(1 - \frac{\rho}{\rho_{open}} \left(\frac{1}{1 - A/A_{open}}\right)\right)} \quad (14)$$

To further simplify, we assume,

$$\frac{L}{L_{open}} = \left(\frac{V}{V_{open}}\right)^\gamma$$

and,

$$\frac{A}{A_{open}} = \left(\frac{V}{V_{open}}\right)^{(1-\gamma)}$$

where  $V$  is the volume of the molecule,  $V_{open}$  is the volume of the open pore, and  $\gamma$  parameterizes the molecule's shape inside the nanopore.  $\gamma \sim 1$  corresponds to a rod shaped molecule and  $\gamma = \frac{1}{3}$  corresponds to a spherical molecule.

The molecular volume ratio can also be written in terms of the molecular weight,  $M$ ,

$$\frac{V}{V_{open}} = \frac{M}{\alpha}$$

where  $\alpha$  is the upper limit of the molecular mass that can enter the nanopore. The resistivity ratio,  $\beta$ , is a more complex parameter that describes ion interactions with the molecule.<sup>28</sup> For simplicity, and because PEG and peptides are near neutral,  $\beta$  will be assumed to be constant.

$$\frac{\rho}{\rho_{open}} = \beta$$

From these simplifications, equation (14) can be simplified to,

$$\frac{\langle i \rangle}{\langle i_0 \rangle} = \frac{1}{1 - \left(\frac{M}{\alpha}\right)^\gamma \left(1 - \beta \left(1 - \left(\frac{M}{\alpha}\right)^{1-\gamma}\right)^{-1}\right)} \quad (15)$$

Fitting the current blockade levels for each peptide with respect to the peptide molecular weights using equation (15), gives the following values,

$$\alpha = 2630 \pm 50 \text{ g/mol}$$

$$\beta = 0.51 \pm 0.01$$

$$\gamma = 0.84 \pm 0.04$$

Fitting the current blockade levels for each PEG data point with respect that the PEG molecular weight using equation (15), give the following values,

$$\alpha = 2760 \pm 70 \text{ g/mol}$$

$$\beta = 1.15 \pm 0.06$$

$$\gamma = 0.69 \pm 0.04$$

These values are consistent with known values. For example, the upper limit cutoff for PEG molecules entering the *trans*-side of a  $\alpha$ -hemolysin pore has been found to be ca. 3000 Daltons.<sup>79</sup>

The least-squares fitted parameter for  $\gamma$  is nearly 1 which is consistent with molecules forming

somewhat rod-like structures in the *trans*-lumen region of the pore. This agreement verifies that the trend seen in Figure 20 is in agreement with a theoretical prediction of molecular weight based on current blockade. A least squares fit can be used to show this trend and potentially be used as a calibration curve for determining unknown molecular weights based on current blockade depth (Figure 30).

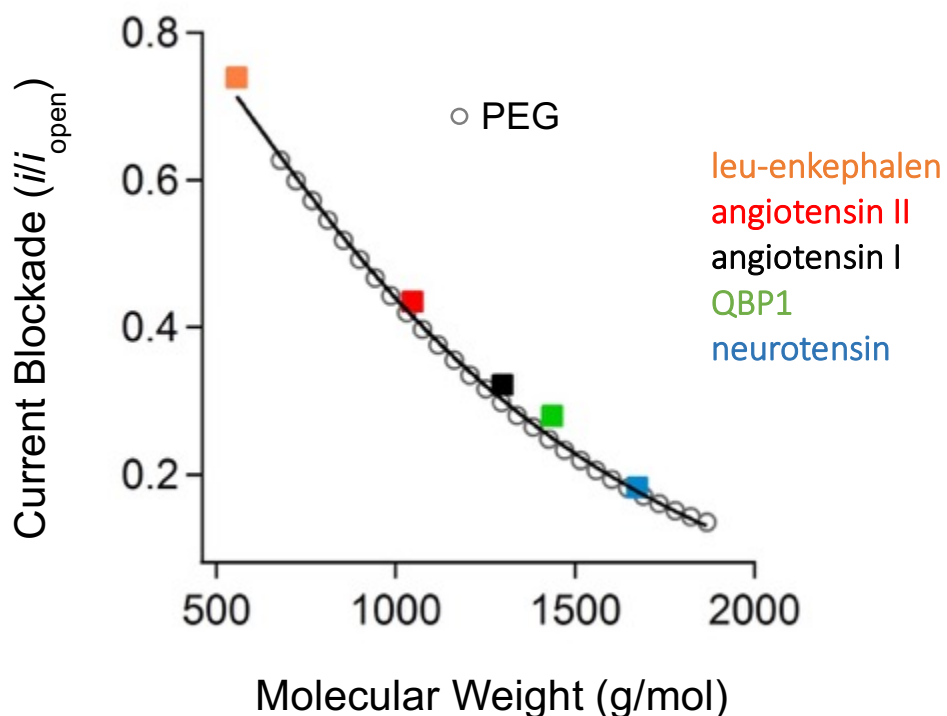


**Figure 30:** A least squares fit showing the trend of current blockade depth and their corresponding molecular weight for PEG (open circles) and peptides (colored squares).

### 4.3. Future Directions

The optimization of PEG residence time using  $\text{Au}_{25}(\text{SG})_{18}$  suggests a way to improve the enhancement by permanently fixing the cluster deep within the nanopore volume.<sup>80</sup> This encourages a stronger interaction when the target analyte is in the *trans*-side lumen. Additionally, if a cluster is fixed within the pore vestibule, the contribution of electroosmotic flow to the residence time enhancement is more easily quantifiable which could lead to further optimization using pH adjustments.<sup>81</sup>

The results from Section 4.1.3. are consistent with the cluster-PEG interaction model of residence time enhancement. This suggests that the simplified Ohmic model (Figure 27), applied to the interaction term ( $d$ ), should enable one to characterize the interaction strength between a metallic cluster and a PEG-like molecule in a nano-confined environment.

When a peptide interacts with a nanopore, the degree of noise is greater than what is observed with PEG (Figure 23). However, changing the pH of solution and adding a denaturing agent like Gdm-HCl decreased the standard deviation when taking the average of these current blockades. This indicates that there is a structural component contributing to this increase in noise, so that SMNS could be used as an alternate method to examine the structural variety between molecules based on their individual blockade characteristics, and peak position.

## 5. CONCLUSION

The experiments conducted in this thesis have demonstrated that nanopore-based resistive pulse sensing is a promising tool for label-free peptide analysis. Previously, it was found that SMNS PEG-based detection is greatly improved when a charged  $\text{Au}_{25}(\text{SG})_{18}$  cluster is present within the *cis*-side region of the pore. A cluster encourages PEG molecules to spend extended periods of time within the pore volume and increases the overall resolution of the current blockade distribution. In this thesis the cluster-PEG interaction was further explored, and optimal voltage conditions for cluster-based residence time enhancement was found to be near 60 mV. The cluster position and orientation within the nanopore was found to have not only an important role in the residence time enhancement but also the mere presence of a cluster improved PEG on-rate to the pore. It was also demonstrated that a cluster-PEG interaction term describing the shift in current blockade distributions can be used to quantify the relative strength of a cluster-polymer interaction.

Additionally, it was demonstrated that SMNS can be used for other analytes. Specifically, PLL exhibited the same characteristic comb-like blockade peaks seen using PEG. Several water soluble peptides were also analyzed using SMNS and gave rise to well-defined and unimodal blockade peaks that distributed consistently with PEG and molecular weight. SMNS peptide sensing was then enhanced with the introduction of a  $\text{Au}_{25}(\text{SG})_{18}$  cluster, altering solution pH, and adding a denaturing agent. Finally, a model is developed that verifies the connection between analyte molecular weight and ionic current blockades.

## 6. REFERENCES

- <sup>1</sup> Majd, S., Yusko, E. C., Billeh, Y. N., Macrae, M. X., Yang, J., & Mayer, M. (2010). Applications of biological pores in nanomedicine, sensing, and nanoelectronics. *Current opinion in biotechnology*, 21(4), 439-476.
- <sup>2</sup> Steffensen, M. B., Rotem, D., & Bayley, H. (2014). Single-molecule analysis of chirality in a multicomponent reaction network. *Nature chemistry*, 6(7), 603-607.
- <sup>3</sup> Jain, K. K. (2007). Applications of nanobiotechnology in clinical diagnostics. *Clinical chemistry*, 53(11), 2002-2009.
- <sup>4</sup> Yáñez-Sedeño, P., Agüí, L., Villalonga, R., & Pingarrón, J. M. (2014). Biosensors in forensic analysis. A review. *Analytica chimica acta*, 823, 1-19.
- <sup>5</sup> Keyser, U. F. (2011). Controlling molecular transport through nanopores. *Journal of The Royal Society Interface*, rsif20110222.
- <sup>6</sup> Coulter, Wallace H. "Means for counting particles suspended in a fluid." U.S. Patent 2,656,508, issued October 20, 1953.
- <sup>7</sup> Bayley, H., & Martin, C. R. (2000). Resistive-pulse sensing from microbes to molecules. *Chemical Reviews*, 100(7), 2575-2594.
- <sup>8</sup> Song, L., Hobaugh, M. R., Shustak, C., Cheley, S., Bayley, H., & Gouaux, J. E. (1996). Structure of staphylococcal  $\alpha$ -hemolysin, a heptameric transmembrane pore. *Science*, 274(5294), 1859-1865.
- <sup>9</sup> Kasianowicz, J. J., Burden, D. L., Han, L. C., Cheley, S., & Bayley, H. (1999). Genetically engineered metal ion binding sites on the outside of a channel's transmembrane  $\beta$ -barrel. *Biophysical journal*, 76(2), 837-845.
- <sup>10</sup> DeGuzman, V. S., Lee, C. C., Deamer, D. W., & Vercoutere, W. A. (2006). Sequence-dependent gating of an ion channel by DNA hairpin molecules. *Nucleic acids research*, 34(22), 6425-6437.
- <sup>11</sup> Schmidt, J. (2016). Membrane platforms for biological nanopore sensing and sequencing. *Current Opinion in Biotechnology*, 39, 17-27.

- 
- 12 Mueller, P., Rudin, D. O., Ti Tien, H., & Wescott, W. C. (1962). Reconstitution of cell membrane structure in vitro and its transformation into an excitable system. *Nature*, *194*, 979-980.
- 13 Mueller, P., Rudin, D. O., Tien, H. T., & Wescott, W. C. (1963). Methods for the formation of single bimolecular lipid membranes in aqueous solution. *The Journal of Physical Chemistry*, *67*(2), 534-535.
- 14 Castellana, E. T., & Cremer, P. S. (2006). Solid supported lipid bilayers: From biophysical studies to sensor design. *Surface Science Reports*, *61*(10), 429-444.
- 15 Kasianowicz, J. J., Balijepalli, A. K., Etedgui, J., Forstater, J. H., Wang, H., Zhang, H., & Robertson, J. W. (2015). Analytical applications for pore-forming proteins. *Biochimica et Biophysica Acta (BBA)-Biomembranes*.
- 16 Quick, J., Loman, N. J., Duraffour, S., Simpson, J. T., Severi, E., Cowley, L., ... & Ouédraogo, N. (2016). Real-time, portable genome sequencing for Ebola surveillance. *Nature*, *530*(7589), 228-232.
- 17 Wang, Y., Zheng, D., Tan, Q., Wang, M. X., & Gu, L. Q. (2011). Nanopore-based detection of circulating microRNAs in lung cancer patients. *Nature nanotechnology*, *6*(10), 668-674.
- 18 Manrao, E. A., Derrington, I. M., Laszlo, A. H., Langford, K. W., Hopper, M. K., Gillgren, N., ... & Gundlach, J. H. (2012). Reading DNA at single-nucleotide resolution with a mutant MspA nanopore and phi29 DNA polymerase. *Nature biotechnology*, *30*(4), 349-353.
- 19 Hu, Y. X., Ying, Y. L., Gu, Z., Cao, C., Yan, B. Y., Wang, H. F., & Long, Y. T. (2016). Single molecule study of initial structural features on the amyloidosis process. *Chemical Communications*, *52*(32), 5542-5545.
- 20 Nivala, J., Marks, D. B., & Akeson, M. (2013). Unfoldase-mediated protein translocation through an [alpha]-hemolysin nanopore. *Nature biotechnology*, *31*(3), 247-250.
- 21 Kasianowicz, J. J., Robertson, J. W., Chan, E. R., Reiner, J. E., & Stanford, V. M. (2008). Nanoscopic porous sensors. *Annu. Rev. Anal. Chem.*, *1*, 737-766.
- 22 Krasilnikov, O. V., Sabirov, R. Z., Ternovsky, V. I., Merzliak, P. G., & Muratkhodjaev, J. N. (1992). A simple method for the determination of the pore radius of ion channels in planar lipid bilayer membranes. *FEMS microbiology immunology*, *5*(1-3), 93-100.
- 23 Merzlyak, P. G., Yuldasheva, L. N., Rodrigues, C. G., Carneiro, C. M., Krasilnikov, O. V., & Bezrukov, S. M. (1999). Polymeric nonelectrolytes to probe pore geometry: application to the  $\alpha$ -toxin transmembrane channel. *Biophysical journal*, *77*(6), 3023-3033.

- 
- <sup>24</sup> Krasilnikov, O. V., Rodrigues, C. G., & Bezrukov, S. M. (2006). Single polymer molecules in a protein nanopore in the limit of a strong polymer-pore attraction. *Physical review letters*, *97*(1), 018301.
- <sup>25</sup> Robertson, J. W., Rodrigues, C. G., Stanford, V. M., Rubinson, K. A., Krasilnikov, O. V., & Kasianowicz, J. J. (2007). Single-molecule mass spectrometry in solution using a solitary nanopore. *Proceedings of the National Academy of Sciences*, *104*(20), 8207-8211.
- <sup>26</sup> Rodrigues, C. G., Machado, D. C., Chevtchenko, S. F., & Krasilnikov, O. V. (2008). Mechanism of KCl enhancement in detection of nonionic polymers by nanopore sensors. *Biophysical journal*, *95*(11), 5186-5192.
- <sup>27</sup> Baaken, G., Ankri, N., Schuler, A. K., Rhe, J., & Behrends, J. C. (2011). Nanopore-based single-molecule mass spectrometry on a lipid membrane microarray. *Acs Nano*, *5*(10), 8080-8088.
- <sup>28</sup> Reiner, J. E., Kasianowicz, J. J., Nablo, B. J., & Robertson, J. W. (2010). Theory for polymer analysis using nanopore-based single-molecule mass spectrometry. *Proceedings of the National Academy of Sciences*, *107*(27), 12080-12085.
- <sup>29</sup> Harris, J. M. (Ed.). (2013). *Poly (ethylene glycol) chemistry: biotechnical and biomedical applications*. Springer Science & Business Media.
- <sup>30</sup> Veronese, F. M. (2001). Peptide and protein PEGylation: a review of problems and solutions. *Biomaterials*, *22*(5), 405-417.
- <sup>31</sup> Knop, K., Hoogenboom, R., Fischer, D., & Schubert, U. S. (2010). Poly (ethylene glycol) in drug delivery: pros and cons as well as potential alternatives. *Angewandte Chemie International Edition*, *49*(36), 6288-6308.
- <sup>32</sup> Chen, J., Spear, S. K., Huddleston, J. G., & Rogers, R. D. (2005). Polyethylene glycol and solutions of polyethylene glycol as green reaction media. *Green Chemistry*, *7*(2), 64-82.
- <sup>33</sup> Karakoti, A. S., Das, S., Thevuthasan, S., & Seal, S. (2011). PEGylated inorganic nanoparticles. *Angewandte Chemie International Edition*, *50*(9), 1980-1994.
- <sup>34</sup> Luo, C., Zhang, Y., Zeng, X., Zeng, Y., & Wang, Y. (2005). The role of poly (ethylene glycol) in the formation of silver nanoparticles. *Journal of colloid and interface science*, *288*(2), 444-448.
- <sup>35</sup> Benaglia, M., Puglisi, A., & Cozzi, F. (2003). Polymer-supported organic catalysts. *Chemical reviews*, *103*(9), 3401-3430.

- 
- <sup>36</sup> Wuelfing, W. P., Gross, S. M., Miles, D. T., & Murray, R. W. (1998). Nanometer gold clusters protected by surface-bound monolayers of thiolated poly (ethylene glycol) polymer electrolyte. *Journal of the American Chemical Society*, *120*(48), 12696-12697.
- <sup>37</sup> Templeton, A. C., Wuelfing, W. P., & Murray, R. W. (2000). Monolayer-protected cluster molecules. *Accounts of Chemical Research*, *33*(1), 27-36.
- <sup>38</sup> Li, W., Bell, N. A., Hernández-Ainsa, S., Thacker, V. V., Thackray, A. M., Bujdoso, R., & Keyser, U. F. (2013). Single protein molecule detection by glass nanopores. *ACS nano*, *7*(5), 4129-4134.
- <sup>39</sup> Han, A., Schürmann, G., Mondin, G., Bitterli, R. A., Hegelbach, N. G., de Rooij, N. F., & Stauer, U. (2006). Sensing protein molecules using nanofabricated pores. *Applied Physics Letters*, *88*(9), 3901.
- <sup>40</sup> Cressiot, B., Oukhaled, A., Patriarche, G., Pastoriza-Gallego, M., Betton, J. M., Auvray, L., ... & Pelta, J. (2012). Protein transport through a narrow solid-state nanopore at high voltage: experiments and theory. *ACS nano*, *6*(7), 6236-6243.
- <sup>41</sup> Hornblower, B., Coombs, A., Whitaker, R. D., Kolomeisky, A., Picone, S. J., Meller, A., & Akeson, M. (2007). Single-molecule analysis of DNA-protein complexes using nanopores. *Nature Methods*, *4*(4), 315-317.
- <sup>42</sup> Sutherland, T. C., Long, Y. T., Stefureac, R. I., Bediako-Amoa, I., Kraatz, H. B., & Lee, J. S. (2004). Structure of peptides investigated by nanopore analysis. *Nano letters*, *4*(7), 1273-1277.
- <sup>43</sup> Wu, D., Bi, S., Zhang, L., & Yang, J. (2014). Single-molecule study of proteins by biological nanopore sensors. *Sensors*, *14*(10), 18211-18222.
- <sup>44</sup> Zhao, Q., de Zoysa, R. S. S., Wang, D., Jayawardhana, D. A., & Guan, X. (2009). Real-time monitoring of peptide cleavage using a nanopore probe. *Journal of the American Chemical Society*, *131*(18), 6324-6325.
- <sup>45</sup> Zhou, S., Wang, L., Chen, X., & Guan, X. (2016). Label-free nanopore single-molecule measurement of trypsin activity. *ACS Sensors*.
- <sup>46</sup> Uhlig, T., Kyprianou, T., Martinelli, F. G., Oppici, C. A., Heiligers, D., Hills, D., ... & Verhaert, P. (2014). The emergence of peptides in the pharmaceutical business: From exploration to exploitation. *EuPA Open Proteomics*, *4*, 58-69.
- <sup>47</sup> Seo, M. D., Won, H. S., Kim, J. H., Mishig-Ochir, T., & Lee, B. J. (2012). Antimicrobial peptides for therapeutic applications: a review. *Molecules*, *17*(10), 12276-12286.
- <sup>48</sup> Movileanu, L., Schmittschmitt, J. P., Scholtz, J. M., & Bayley, H. (2005). Interactions of peptides with a protein pore. *Biophysical journal*, *89*(2), 1030-1045.

- 
- 49 Goodrich, C. P., Kirmizialtin, S., Huyghues-Despointes, B. M., Zhu, A., Scholtz, J. M., Makarov, D. E., & Movileanu, L. (2007). Single-molecule electrophoresis of  $\beta$ -hairpin peptides by electrical recordings and Langevin dynamics simulations. *The Journal of Physical Chemistry B*, *111*(13), 3332-3335.
- 50 Oukhaled, G., Mathe, J., Biance, A. L., Bacri, L., Betton, J. M., Lairez, D., ... & Auvray, L. (2007). Unfolding of proteins and long transient conformations detected by single nanopore recording. *Physical review letters*, *98*(15), 158101.
- 51 Saborio, G. P., Permanne, B., & Soto, C. (2001). Sensitive detection of pathological prion protein by cyclic amplification of protein misfolding. *Nature*, *411*(6839), 810-813.
- 52 Wang, H. Y., Gu, Z., Cao, C., Wang, J., & Long, Y. T. (2013). Analysis of a single  $\alpha$ -synuclein fibrillation by the interaction with a protein nanopore. *Analytical chemistry*, *85*(17), 8254-8261.
- 53 Hu, Z. L., Cao, C., Wang, H. F., & Yan, B. Y. (2016). Alkyl detection facilitated by a DNA conjugate with an  $\alpha$ -hemolysin nanopore. *RSC Advances*, *6*(1), 105-108.
- 54 Fologea, D., Uplinger, J., Thomas, B., McNabb, D. S., & Li, J. (2005). Slowing DNA translocation in a solid-state nanopore. *Nano letters*, *5*(9), 1734-1737.
- 55 Kowalczyk, S. W., Wells, D. B., Aksimentiev, A., & Dekker, C. (2012). Slowing down DNA translocation through a nanopore in lithium chloride. *Nano letters*, *12*(2), 1038-1044.
- 56 Berg, H. C., & Purcell, E. M. (1977). Physics of chemoreception. *Biophysical journal*, *20*(2), 193.
- 57 Angevine, C. E., Chavis, A. E., Kothalawala, N., Dass, A., & Reiner, J. E. (2014). Enhanced single molecule mass spectrometry via charged metallic clusters. *Analytical chemistry*, *86*(22), 11077-11085.
- 58 Heaven, M. W., Dass, A., White, P. S., Holt, K. M., & Murray, R. W. (2008). Crystal structure of the gold nanoparticle [N (C<sub>8</sub>H<sub>17</sub>)<sub>4</sub>][Au<sub>25</sub> (SCH<sub>2</sub>CH<sub>2</sub>Ph)<sub>18</sub>]. *Journal of the American Chemical Society*, *130*(12), 3754-3755.
- 59 Zhu, M., Aikens, C. M., Hollander, F. J., Schatz, G. C., & Jin, R. (2008). Correlating the crystal structure of a thiol-protected Au<sub>25</sub> cluster and optical properties. *Journal of the American Chemical Society*, *130*(18), 5883-5885.
- 60 Shichibu, Y., Negishi, Y., Tsunoyama, H., Kanehara, M., Teranishi, T., & Tsukuda, T. (2007). Extremely High Stability of Glutathionate-Protected Au<sub>25</sub> Clusters Against Core Etching. *Small*, *3*(5), 835-839.

- 
- <sup>61</sup> Xie, S., Tsunoyama, H., Kurashige, W., Negishi, Y., & Tsukuda, T. (2012). Enhancement in aerobic alcohol oxidation catalysis of Au<sub>25</sub> clusters by single Pd atom doping. *ACS Catalysis*, 2(7), 1519-1523.
- <sup>62</sup> Liu, Y., Tsunoyama, H., Akita, T., & Tsukuda, T. (2010). Efficient and selective epoxidation of styrene with TBHP catalyzed by Au<sub>25</sub> clusters on hydroxyapatite. *Chemical Communications*, 46(4), 550-552.
- <sup>63</sup> Zhu, Y., Qian, H., Drake, B. A., & Jin, R. (2010). Atomically Precise Au<sub>25</sub> (SR) 18 Nanoparticles as Catalysts for the Selective Hydrogenation of  $\alpha$ ,  $\beta$ -Unsaturated Ketones and Aldehydes. *Angewandte Chemie*, 122(7), 1317-1320.
- <sup>64</sup> Zhu, M., Aikens, C. M., Hendrich, M. P., Gupta, R., Qian, H., Schatz, G. C., & Jin, R. (2009). Reversible switching of magnetism in thiolate-protected Au<sub>25</sub> superatoms. *Journal of the American Chemical Society*, 131(7), 2490-2492.
- <sup>65</sup> Huck, W. T. (2005). Effects of nanoconfinement on the morphology and reactivity of organic materials. *Chemical communications*, (33), 4143-4148.
- <sup>66</sup> Kothalawala, N., West IV, J. L., & Dass, A. (2014). Size-dependent molecule-like to plasmonic transition in water-soluble glutathione stabilized gold nanomolecules. *Nanoscale*, 6(2), 683-687.
- <sup>67</sup> Menestrina, G. (1986). Ionic channels formed by *Staphylococcus aureus* alpha-toxin: Voltage-dependent inhibition by divalent and trivalent cations. *The Journal of membrane biology*, 90(2), 177-190.
- <sup>68</sup> Balijepalli, A., Robertson, J. W., Reiner, J. E., Kasianowicz, J. J., & Pastor, R. W. (2013). Theory of Polymer–Nanopore Interactions Refined Using Molecular Dynamics Simulations. *Journal of the American Chemical Society*, 135(18), 7064-7072.
- <sup>69</sup> Chavis, A. E., Brady, K. T., Kothalawala, N., & Reiner, J. E. (2015). Voltage and blockade state optimization of cluster-enhanced nanopore spectrometry. *Analyst*, 140(22), 7718-7725.
- <sup>70</sup> Breton, M. F., Discala, F., Bacri, L., Foster, D., Pelta, J., & Oukhaled, A. (2013). Exploration of neutral versus polyelectrolyte behavior of poly (ethylene glycol) s in alkali ion solutions using single-nanopore recording. *The Journal of Physical Chemistry Letters*, 4(13), 2202-2208.
- <sup>71</sup> Rodrigues, C. G., Machado, D. C., Chevchenko, S. F., & Krasilnikov, O. V. (2008). Mechanism of KCl enhancement in detection of nonionic polymers by nanopore sensors. *Biophysical journal*, 95(11), 5186-5192.

- 
- 72 Campos, E., McVey, C. E., Carney, R. P., Stellacci, F., Astier, Y., & Yates, J. (2013). Sensing Single Mixed-Monolayer Protected Gold Nanoparticles by the  $\alpha$ -Hemolysin Nanopore. *Analytical chemistry*, 85(21), 10149-10158.
- 73 Oukhaled, A., Cressiot, B., Bacri, L., Pastoriza-Gallego, M., Betton, J. M., Bourhis, E., ... & Pelta, J. (2011). Dynamics of completely unfolded and native proteins through solid-state nanopores as a function of electric driving force. *ACS nano*, 5(5), 3628-3638.
- 74 Rosenstein, J. K., Wanunu, M., Merchant, C. A., Drndic, M., & Shepard, K. L. (2012). Integrated nanopore sensing platform with sub-microsecond temporal resolution. *Nature methods*, 9(5), 487-492.
- 75 Uram, J. D., Ke, K., & Mayer, M. (2008). Noise and bandwidth of current recordings from submicrometer pores and nanopores. *ACS nano*, 2(5), 857-872.
- 76 Mirtič, A., & Grdadolnik, J. (2013). The structure of poly-l-lysine in different solvents. *Biophysical chemistry*, 175, 47-53.
- 77 Israelachvili, J. N. (2011). *Intermolecular and surface forces: revised third edition*. Academic press.
- 78 Aksimentiev, A., & Schulten, K. (2005). Imaging  $\alpha$ -hemolysin with molecular dynamics: ionic conductance, osmotic permeability, and the electrostatic potential map. *Biophysical journal*, 88(6), 3745-3761.
- 79 Bayley, H. (1994). Triggings and switches in a self-assembling pore-forming protein. *Journal of cellular biochemistry*, 56(2), 177-182.
- 80 Bayley, H. (1994). Triggings and switches in a self-assembling pore-forming protein. *Journal of cellular biochemistry*, 56(2), 177-182.
- 81 Mereuta, L., Asandei, A., Seo, C. H., Park, Y., & Luchian, T. (2014). Quantitative Understanding of pH- and Salt-Mediated Conformational Folding of Histidine-Containing,  $\beta$ -Hairpin-Like Peptides, through Single-Molecule Probing with Protein Nanopores. *ACS applied materials & interfaces*, 6(15), 13242-13256.